ISSN 0869-5911, Petrology, 2006, Vol. 14, No. 4, pp. 337–360. © Pleiades Publishing, Inc., 2006.
Original Russian Text © A.M. Kozlovsky, V.V. Yarmolyuk, V.M. Savatenkov, V.P. Kovach, 2006, published in Petrologiya, 2006, Vol. 14, No. 4, pp. 358–383.

Sources of Basaltoid Magmas in Rift Settings of an Active Continental Margin: Example from the Bimodal Association of the Noen and Tost Ranges of the Late Paleozoic Gobi–Tien Shan Rift Zone, Southern Mongolia

A. M. Kozlovsky[a], V. V. Yarmolyuk[a], V. M. Savatenkov[b], and V. P. Kovach[b]

[a] *Institute of Geology of Ore Deposits, Petrography, Mineralogy, and Geochemistry (IGEM), Russian Academy of Sciences, Staromonetnyi per. 35, Moscow, 119017 Russia*

e-mail: amk@igem.ru

[b] *Institute of Precambrian Geology and Geochronology, Russian Academy of Sciences, nab. Makarova 2, St. Petersburg, 199034 Russia*

Received May 11, 2005

Abstract—The bimodal volcanoplutonic (basalt–peralkaline rhyolite with peralkaline granites) association of the Noen and Tost ranges was formed 318 Ma ago in the Gobi–Tien Shan rift zone of the Late Paleozoic–Early Mesozoic central Asian rift system, the development of which was related to the movement of the continental lithosphere over a mantle hot spot. A specific feature of the Late Paleozoic rifting was that it occurred within the Middle–Late Paleozoic active continental margin of the northern Asian paleocontinent. Continental margin magmatism was followed after a short time delay by the magmatism of the Gobi–Tien Shan rift zone, which was located directly in the margin of the paleocontinent. Such a geodynamic setting of the rift zone was reflected in the geochemical characteristics of rift-related rocks. The distribution of major elements and compatible trace elements in the rift-related basic and intermediate rocks corresponds to a crystallization differentiation series. The distribution of incompatible trace elements suggests contributions from several sources. This is also supported by the heterogeneity of Sr and Nd isotopic compositions of the rift-related basaltoids: $\varepsilon_{Nd}(T)$ ranges from 4.4 to 6.7, and $(^{87}Sr/^{86}Sr)_0$, from 0.70360 to 0.70427. The geochemical characteristics of the rift-related basaltoids of the Noen and Tost ranges are not typical of rift settings (negative anomalies in Nb and Ta and positive anomalies in K and Pb) and suggest a significant role of the rocks of a metasomatized mantle wedge in their source. In addition, there are high-titanium rocks among the rift-related basaltoids, whose geochemical characteristics approach those of the basalts of mid-ocean ridges and ocean islands. This allowed us to conclude that the compositional variations of the rift-related basaltoids of the Noen and Tost ranges were controlled by three magma sources: the enriched mantle, depleted mantle (high-titanium basaltoids), and metasomatized mantle wedge (medium-Ti basaltoids). The medium-titanium basaltoids were formed in equilibrium with spinel peridotites, whereas the high-titanium magmas were formed at deeper levels both in the spinel and garnet zones. It terms of geodynamics, the occurrence of three sources of the rift-related basaltoids of the Noen and Tost ranges was related to the ascent of a mantle plume with enriched geochemical characteristics beneath a continental margin, where its influence caused melting in the overlying depleted mantle and the metasomatized mantle wedge. The formation of rift-related andesites in the Noen and Tost ranges was explained by the contamination of mantle-derived basaltoid melts with sialic (mainly sedimentary) continental crustal materials or the assimilation of anatectic granitoid melts.

DOI: 10.1134/S0869591106040023

INTRODUCTION

During the Late Paleozoic and Early Mesozoic, one of the world's largest rift systems was formed in the central Asian fold belt (Yarmolyuk, 1983). One specific feature of its tectonic setting is that it developed within the Middle–Late Paleozoic active continental margin (ACM) of the northern Asian paleocontinent (Gordienko, 1987; *Tectonics, Magmatism…*, 2001). The processes of rift formation postdated with a short time break the magmatism of the ACM and were superimposed on the structures of the marginal volcanic belt. The structure of the rift system is built up by a series of near-parallel rift zones (from south to north: Gobi–Tien Shan, main Mongolian lineament, Gobi–Altai, northern Mongolian, and western Transbaikalian), the age of which decreases sequentially from the margin to the interior of the continent: from the Late Carboniferous in the southern part of the rift system to the Late Permian and Early Mesozoic in its northern part. Such a peculiar development of the rift system is explained by the gradual movement of the continental plate over a mantle hot spot, which initiated the processes of rifting (Yarmolyuk et al., 1999; Yarmolyuk and Kovalenko, 2000).

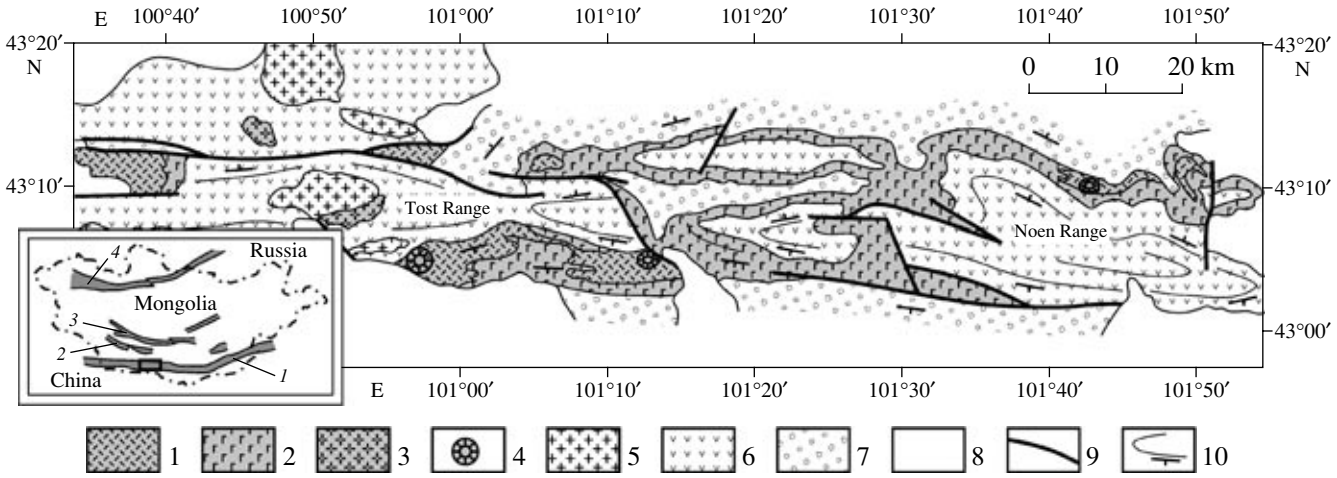

Fig. 1. Sketch map showing the geological structure of the bimodal volcanoplutonic association of the graben of the Tost and Noen ranges. (1)–(4) Rocks of the bimodal association: (1) peralkaline rhyolite, (2) basaltoid and andesite, (3) peralkaline granite, and (4) vent rock; (5) biotite granite; (6) underlying Carboniferous volcanic rocks of the active continental margin complex; (7) overlying Permian and Triassic conglomerate; (8) unconsolidated deposit; (9) fault; and (10) boundaries of sheets and sequences and their strikes and dips. The inset shows the position of the Late Paleozoic rift zones in the territory of Mongolia and adjacent areas. Rift zones: *1*, Gobi–Tien Shan; *2*, Main Mongolian lineament; *3*, Gobi–Altai; and *4*, northern Mongolia. The region of the Noen and Tost ranges is indicated by the rectangle.

Although the magmatism of the central Asian rift system is similar to that of typical intracontinental rift zones, such as the East African rift, Tunisian rift, and others (Peccerillo et al., 2003; Trua et al., 1999; Civetta et al., 1998; Barberi et al., 1975; Davies and Macdonald, 1987), and represented by bimodal basalt–peralkaline rhyolite volcanic associations with peralkaline granites, the occurrence of rift-forming processes at a convergent plate boundary affected the compositions of rift-related rocks.

This paper addresses some problems of the petrogenesis of basic and intermediate rocks from the rift-related bimodal association belonging to the Gobi–Tien Shan rift zone, which is the oldest in the rift system and was formed directly near the margin of the northern Asian paleocontinent. The rift zone extends in the E–W direction throughout southern Mongolia over a distance of more than 1000 km and is marked in the modern erosion level by a system of closely spaced near-parallel faults, chains of grabens filled with volcanic rocks of the bimodal association, belts of parallel dikes, and peralkaline granitoid massifs. One of the largest grabens is situated in the western part of the rift zone and is connected in modern topography with the Noen and Tost ranges of the Gobi Tien Shan.

GEOLOGY OF THE REGION OF THE NOEN AND TOST RANGES

The graben of the Noen and Tost ranges is traced over a distance of more than 200 km at a width of 30–40 km (Fig. 1) and is filled with the rocks of the bimodal volcanic basalt–peralkaline rhyolite association associating with peralkaline granite bodies (Yarmolyuk, 1978; Yarmolyuk and Kovalenko, 1991). The graben is embedded in the structures of the ACM volcanic belt, which includes Early–Middle Carboniferous fields of lavas, tuff lavas, ignimbrites, and welded tuffs of basalts, basaltic andesites, andesites, dacites, and rhyolites metamorphosed to greenschist facies conditions. In places, tuff–sedimentary members, up to 400 m thick, were documented between the ACM complexes and the volcanic sequences of the bimodal association. The rocks of the bimodal association are overlain by Permian–Triassic conglomerates and Mesozoic–Cenozoic cover deposits. The whole PZ_3–MZ_1 complex was affected by dislocations forming a system of large E–W trending folds, which resulted in that the volcanic sequences of the Noen–Tost graben appeared in the axial part of a large anticline. The rocks of the ACM complex are exposed in the core of the anticline, where they are intruded by bodies of normal and peralkaline granitoids and dikes of the rift-related complex. The slopes of the anticline are composed of bimodal volcanics.

The volcanic sequence of the bimodal association includes sheet and vent complexes, which are best preserved on the southern and southeastern slopes of the Tost Range (Fig. 2). The following sequence of volcanic facies is observed in this area from the western to the eastern margin of the volcanic field. Near Takhilga-Ula Mount, which corresponds to the vent of a paleovolcano, the volcanic section is dominated by peralkaline rhyolites. They form a series of southeast-dipping steep (up to 30°–40°) flows, up to 30–40 m thick, composed mainly of lavas and ignimbrites, occasionally of lava breccias, tuff lavas, and tuffs. Lenses of basic lavas, up to 50 m thick, were found between the bodies

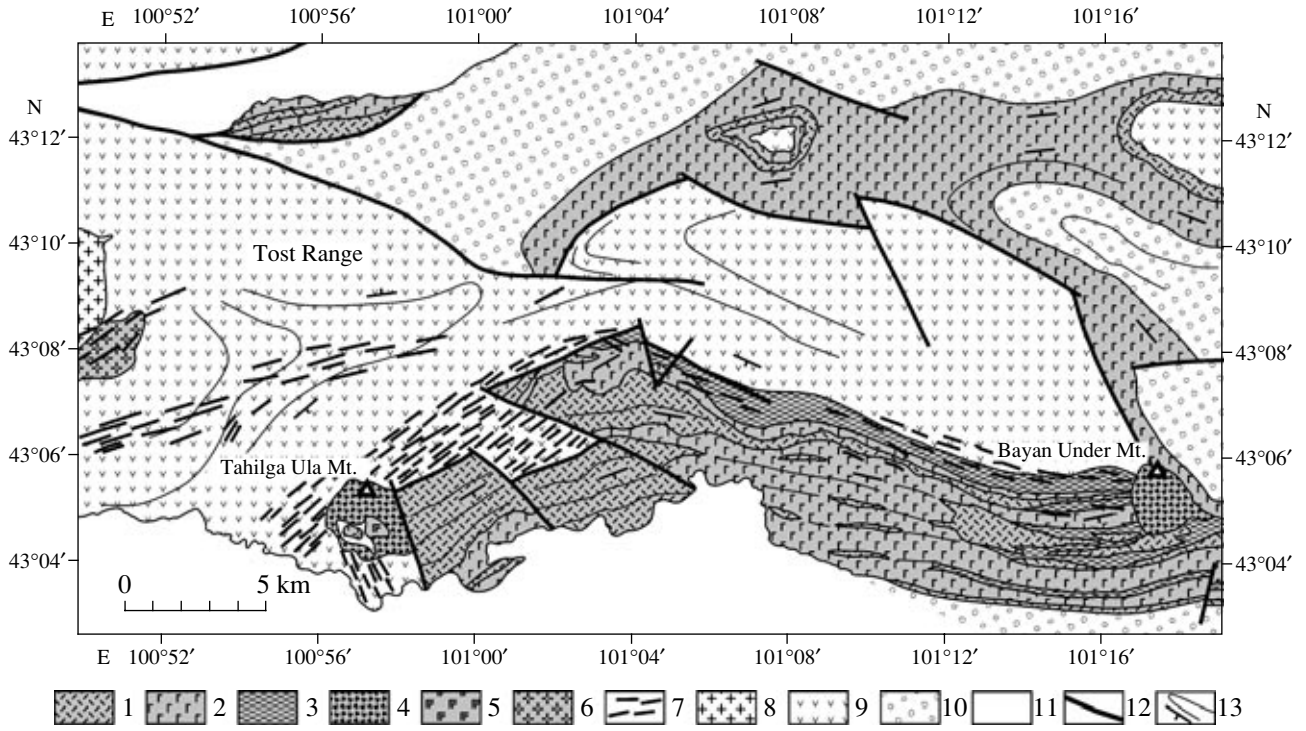

Fig. 2. Simplified geologic structure of the southeastern end of the Tost Range. (1)–(7) Rocks of the bimodal association: (1) peralkaline rhyolite, (2) basaltoid and andesite, (3) tuff–sedimentary rock, (4) vent peralkaline rhyolite, (5) vent basaltoid, (6) peralkaline granite, and (7) dike; (8) biotite granite; (9) underlying Carboniferous volcanic rocks of the active continental margin complex; (10) overlying Permian and Triassic conglomerate; (11) unconsolidated MZ_2–KZ deposits; (12) fault; and (13) boundaries of sheets and sequences and their strikes and dips.

of silicic volcanic rocks. The total thickness of the volcanic sequence in this region is about 1500 m, silicic volcanic rocks account for about 1300 m of this section.

Away from the center of the paleovolcano, the fraction of basic rocks in the section gradually increases at the expense of silicic rocks. As a result, the sequence of alkaline salic rocks pinches out, and only small lenses of such rocks were found far from the volcano among basic volcanics. The later are predominant in this area and account for about 1600 m out of a total thickness of the lava pile of 1800 m. In the eastern part of the lava field, the fraction of silicic rocks increases again, and they form large extrusions up to 2×5 m in size near the vent of the Bayan Under paleovolcano. The amount of tuff–sedimentary rocks increases sharply in this part of the volcanic field. In general, a similar structure of volcanic sequences with contrasting alternation of peralkaline rhyolite and basaltoid flows was observed along the whole length of the graben. Silicic rocks are spatially confined to paleovents and are products of central eruptions, whereas basic flows are independent of vent structures and were probably produced by fissure eruptions or shield volcanism.

The rift-related complex of the Noen and Tost ranges includes numerous dikes of peralkaline rhyolites and basaltoids. They form belts of parallel dikes often contacting or intersecting at an acute angle; there are both basic dikes intersecting silicic ones and vice versa. Such belts are best exemplified in the southeastern part of the Tost Range, where dikes occur in a band 20 km long and 7 km wide. The basic dikes are a few meters thick, and silicic dikes are up to 10–15 m. The fraction of dikes in the section is up to 30 vol %, and peralkaline rhyolites account for about 80% of all dike bodies. Similar dike belts occur on a smaller scale along the whole graben. The appearance of dike belts in the graben structure clearly indicates regional extension conditions (rifting) accompanying the formation of bimodal associations.

The age of the bimodal magmatic association of the Noen and Tost ranges is constrained by the underlying floristically characterized Early–Middle Carboniferous volcanics of the differentiated ACM belt and the overlying Early Permian–Triassic conglomerate molasses. Plant remnants were discovered in tuff–sedimentary interbeds in the section of the bimodal volcanic association. These findings indicated Late Carboniferous–Early Permian age for the rift-related magmatism (Yarmolyuk et al., 1981). Our geochronological studies of the rift-related magmatism yielded a U–Pb zircon age of 318 ± 1 Ma for the peralkaline granites (Kozlovsky et al., 2005). Within the errors, identical age was obtained from the slope of the Rb–Sr errochron based on the bulk-rock samples of volcanics, dikes, and

peralkaline granites of the bimodal association of the Tost Range (314 ± 5 Ma).

ANALYTICAL METHODS

In order to characterize the basic and intermediate rift-related magmatism, more than 60 rock samples from the bimodal association, dike belt, and ACM volcanic complexes were studied in detail. The concentrations of major elements in the rocks were determined by X-ray fluorescence spectrometry at the Vinogradov Institute of Geochemistry, Siberian Division, Russian Academy of Sciences (Irkutsk).

The rock samples were analyzed by inductively coupled plasma mass spectrometry on a VG Elemental PlasmaQuad 3 instrument at the Institute of Analytical Instrument Making, Russian Academy of Sciences, St. Petersburg. The analytical conditions were reported by Kovalenko et al. (2003). The drift of the relative sensitivity of the instrument was checked by a series of measurements of standard solutions (no more than 5–10 samples) containing heavy metals (Ti, Cr, Ni, Cu, and Pb) and the BCR-1 standard. The instrument was calibrated for REE analysis using a multielement standard solution obtained from Johnson Matthew Company. The relative errors for element concentrations were no higher than 5–10%.

The analysis of Sr and Nd isotopes was performed at the Institute of Precambrian Geology and Geochronology, Russian Academy of Sciences, St. Petersburg. Samples for isotope mass spectrometry were prepared using the procedure described by Savatenkov et al. (2004). Isotopic analysis was carried out on a Finnigan MAT-261 multicollector solid-phase mass spectrometer. The precision of Rb, Sr, Sm, and Nd concentrations calculated from the repeated measurements of the BCR-1 standard was ±0.5%. The total blank was 0.05 ng Rb, 0.2 ng Sr, 0.3 ng Sm, and 0.8 ng Nd. The analysis of the BCR-1 standard (six measurements) yielded the following results: [Sr] = 336.7 ppm, [Rb] = 47.46 ppm, [Sm] = 6.47 ppm, [Nd] = 28.13 ppm, $^{87}Rb/^{86}Sr$ = 0.4062, $^{87}Sr/^{86}Sr$ = 0.705036 ± 22, $^{147}Sm/^{144}Nd$ = 0.1380, and $^{143}Nd/^{144}Nd$ = 0.512642 ± 14. The precision of isotopic analyses was checked by the measurement of the La Jolla and SRM-987 standards. During the period of our measurements, the $^{87}Sr/^{86}Sr$ ratio of the SRM-987 standard was 0.710241 ± 15 (2σ, 10 analyses), and the $^{143}Nd/^{144}Nd$ ratio of the La Jolla standard was 0.511858 ± 8 (2σ, 12 measurements). The Sr and Nd isotope compositions were normalized to $^{88}Sr/^{86}Sr$ = 8.37521 and $^{148}Nd/^{144}Nd$ = 0.24157.

The oxygen isotope ratios of silicate rocks were determined at the Far East Geological Institute, Far East Division, Russian Academy of Sciences (analysts T.A. Velivetskaya and A.V. Ignat'ev). The measurements were performed on a Finnigan MAT-252 mass spectrometer. The accuracy of $\delta^{18}O$ determination was ±0.1‰ at the 95% confidence level. The $\delta^{18}O$ values are given relative to SMOW.

PETROGRAPHIC CHARACTERISTICS OF BASALTOIDS FROM THE NOEN AND TOST RANGES

Lavas are dominant among the basaltoids of the bimodal association of the Noen and Tost ranges. The rocks are usually porphyritic with a trachytoid distribution of plagioclase laths, euhedral, often twinned clinopyroxene crystals, and scarce titanomagnetite phenocrysts. In addition, there are olivine phenocrysts completely pseudomorphed by secondary minerals. Such phenocrysts often form glomeroporphyric intergrowths with pyroxene. The phenocrysts of mafic minerals are usually no larger than 1.5 mm, plagioclase is up to 5 mm in size, and the total content of phenocrysts is up to 10%. Aphiric rocks were occasionally found among basic lavas. The groundmass of rocks is finely crystallized with distinct microlites of plagioclase, clinopyroxene, olivine, and an opaque mineral. The compositions of clinopyroxene, plagioclase, and titanomagnetite phenocrysts vary irregularly within the whole range of basic rocks. The clinopyroxene is rather uniform and corresponds to augite, and the composition of plagioclase phenocrysts ranges widely from An_{86} to An_{38}.

CHEMICAL COMPOSITION OF ROCKS

Major Element

The rocks of the bimodal association of the Noen and Tost ranges contain from 47.6 to 78.4 wt % SiO_2 (Fig. 3a) (hereafter, the concentrations of major elements are given in weight percent recalculated to a total of 100% on a volatile-free basis). However, the overwhelming majority of rocks fall into SiO_2 ranges of 47.6–60% and 70–78.4%, i.e., correspond to basaltoids and andesites, on the one hand, and peralkaline rhyolites, on the other. The rocks of transitional compositions occur in very minor amounts. The bimodal distribution of rock compositions is clearly illustrated by the histogram of SiO_2 content (Fig. 3b). It should be taken into account that the histogram was constructed using the results of sampling and does not exactly correspond to the real volume proportions of rocks. This concerns primarily the rocks of intermediate composition, which were difficult to identify during field work and which were therefore sampled more extensively. This paper focuses on the basic and intermediate rocks of the bimodal association of the Noen and Tost ranges containing 48.7–62.7% SiO_2 (Table 1). In the (Na_2O + K_2O)–SiO_2 classification diagram (Le Bas et al., 1986), they plot within the fields of basalt, trachybasalt, basaltic andesite, basaltic trachyandesite (rocks of this group are referred to as basaltoids), andesite, and trachyandesite.

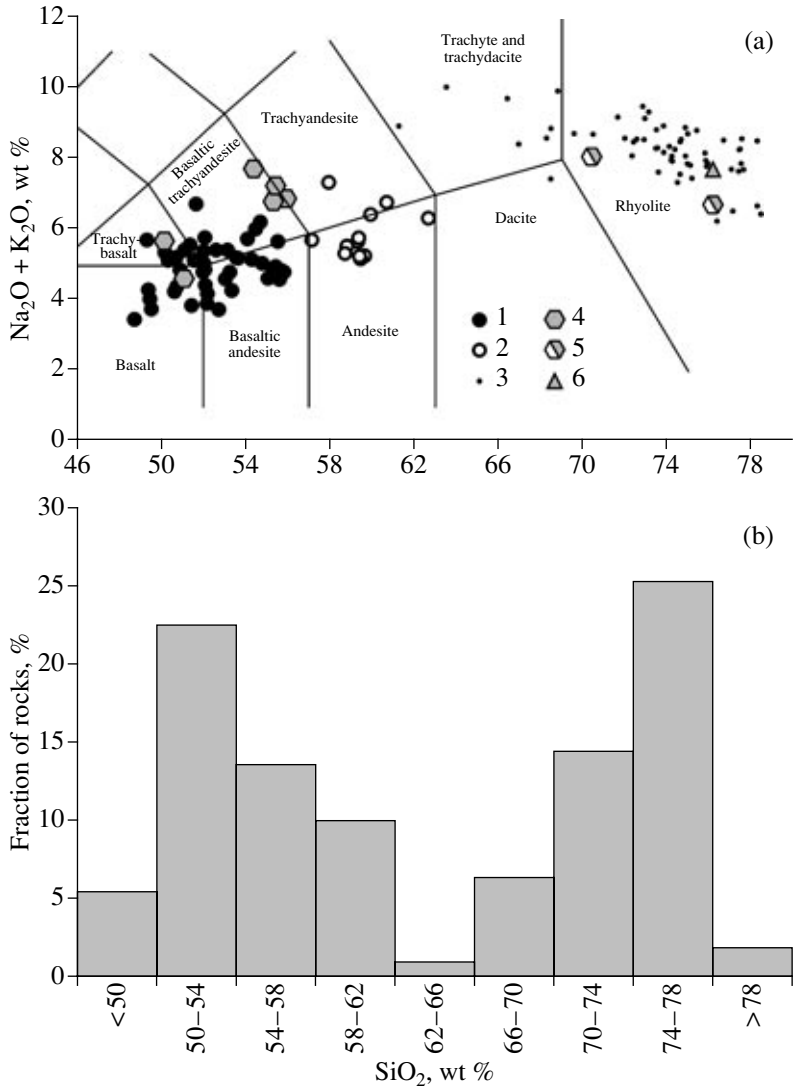

Fig. 3. (a) Total alkali–silica classification diagram (Le Bas et al., 1986) for the rocks of the rift-related bimodal association of the Noen and Tost ranges and the ACM complex and (b) histogram of SiO_2 concentrations in these rocks. (1)–(3) Rocks of the bimodal association: (1) basalt, trachybasalt, basaltic andesite, and basaltic trachyandesite; (2) andesite and trachyandesite; (3) peralkaline rhyolite (our unpublished data); (4) and (5) rocks of the active continental margin complex: (4) basic rock and (5) rhyolite; and (6) biotite granite from the western part of the Tost Range.

In major-element variation diagrams, the compositions of all basic and intermediate rocks of the bimodal association of the Noen and Tost ranges are characterized by negative correlations of SiO_2 with TiO_2, FeO, MgO, CaO, and P_2O_5 (Fig. 4). The concentration of Al_2O_3 is practically independent of SiO_2 and varies from 16 to 19%. Only K_2O exhibits a distinct positive correlation with SiO_2. In general, rocks with similar SiO_2 contents may be significantly different in other elements. This is clearly seen by the example of the distribution of titanium, iron (not shown), sodium, potassium, and phosphorus. The majority of basic rocks of the bimodal association of the Noen and Tost ranges have moderate TiO_2 (<1.6%), FeO (<10.5%), and P_2O_5 (<0.55%) concentrations. There is a small group of relatively high-Ti rocks (up to 2.8% TiO_2), which are also enriched in FeO (up to 12.9%) and P_2O_5 (up to 1%). All the rocks, except for one composition from a basaltic andesite dike and one basaltic flow, have MgO contents below 8% and, consequently, cannot be regarded as direct mantle melts.

The compositions of the rift-related basaltoids are hypersthene-normative (up to 23%). The basalts and trachybasalts contain 4–17% normative olivine. Both olivine- and quartz-normative rocks were found among the basaltic andesites and basaltic trachyandesites. The content of normative quartz in the andesites and trachyandesites is up to 11%.

In the classification diagram (Fig. 3), the basic rocks of the ACM volcanic complex fall, similarly to the

Table 1. Chemical compositions (wt %) of basic rocks from the bimodal association of the Noen and Tost ranges and the ACM complex

Sample no.	Rock	SiO_2	TiO_2	Al_2O_3	FeO	MnO	MgO	CaO	Na_2O	K_2O	P_2O_5	LOI	Total
NT-1/1	B	46.79	2.23	17.02	10.81	0.19	6.61	8.52	2.92	0.43	0.49	3.12	99.13
NT-1/2	B	48.91	1.32	16.71	9.49	0.15	6.48	9.01	2.91	1.22	0.41	2.41	99.02
NT-1/3	TB	48.49	1.39	17.06	9.58	0.16	6.96	7.29	2.73	2.24	0.45	2.56	98.91
NT-1/4	B	49.96	1.27	16.62	9.55	0.14	6.79	8.62	2.82	0.95	0.40	2.04	99.16
NT-1/5	BA	52.03	1.24	16.01	9.06	0.15	5.92	8.49	2.89	1.31	0.43	1.52	99.05
NT-1/6	BTA	50.19	1.29	16.64	9.08	0.15	6.32	7.14	3.07	2.15	0.47	2.58	99.08
NT-1/7	BA	53.90	1.10	17.81	7.78	0.11	4.77	7.50	3.15	1.40	0.38	1.20	99.10
NT-1/8	BA	53.75	1.06	17.25	8.00	0.12	5.15	7.00	3.10	1.52	0.36	1.83	99.14
NT-1/9	TB	49.35	1.58	17.44	9.95	0.14	5.09	8.17	3.93	1.17	0.50	1.69	99.01
NT-1/10	BA	50.40	1.51	16.90	9.51	0.15	5.19	8.14	3.43	1.25	0.47	2.06	99.01
NT-1/11	BA	51.34	1.28	17.29	9.02	0.15	5.45	8.80	3.02	0.65	0.37	1.70	99.07
NT-1/12	BA	50.39	1.48	16.73	9.27	0.15	5.52	8.06	3.65	1.08	0.44	2.30	99.07
NT-1/13	BA	51.52	1.45	16.86	8.97	0.15	5.00	8.22	3.40	1.10	0.45	1.94	99.06
NT-1/14	BA	52.61	1.23	16.51	8.55	0.12	5.00	7.45	3.57	1.45	0.42	2.08	98.99
NT-1/15	BTA	54.20	1.19	16.67	8.09	0.14	4.32	7.01	3.48	2.07	0.43	1.51	99.11
NT-1/16	BA	54.36	1.17	16.74	7.70	0.14	4.56	7.71	3.17	1.57	0.44	1.59	99.15
NT-1/17	BA	52.26	1.28	16.60	8.75	0.15	5.27	7.60	3.41	1.67	0.43	1.73	99.15
NT-1/18	BTA	51.63	1.31	16.94	8.93	0.13	4.89	7.58	3.70	1.59	0.45	1.87	99.02
NT-1/19	BA	53.82	1.05	16.10	7.36	0.11	5.97	7.03	3.27	1.38	0.32	2.92	99.33
NT-1/20	BA	53.57	1.06	16.53	7.61	0.11	5.91	6.90	3.18	1.41	0.34	2.53	99.15
NT-1/21	BA	54.14	1.24	16.93	7.89	0.17	5.36	7.65	3.65	1.36	0.43	0.31	99.13
NT-1/22	BTA	52.97	1.37	16.97	7.70	0.13	4.32	7.32	3.39	2.48	0.60	1.86	99.11
NT-1/23	BTA	52.59	1.44	16.61	7.31	0.12	4.83	8.08	3.83	1.77	0.65	2.00	99.23
NT-1/24	BTA	53.15	1.17	16.81	7.94	0.10	4.78	6.69	3.84	2.22	0.48	2.04	99.22
NT-1/25	BA	54.20	1.19	16.81	8.15	0.15	4.45	7.48	3.47	1.40	0.49	1.44	99.23
NT-2/1	BA	50.36	1.79	16.85	8.67	0.15	5.11	9.24	3.20	0.60	0.55	2.70	99.22
NT-2/2	TA	56.48	1.64	16.62	7.12	0.20	3.07	4.65	5.50	1.67	0.53	1.83	99.31
NT-2/3	TB	48.42	2.39	16.53	9.73	0.30	5.21	8.00	4.37	0.82	0.74	2.44	98.95
NT-2/4	B	48.36	1.40	17.92	9.64	0.16	5.82	10.05	3.33	0.64	0.44	1.32	99.08
NT-2/5	A	57.60	0.92	16.79	6.13	0.12	3.89	6.77	3.37	2.07	0.30	1.45	99.41
NT-2/6	A	58.34	0.90	16.61	7.04	0.09	2.78	6.54	3.14	2.55	0.30	0.93	99.22
NT-2/7	A	55.64	1.08	17.11	6.70	0.10	3.60	7.17	3.39	2.19	0.39	1.81	99.18
NT-2/8	B	49.25	1.57	16.95	9.46	0.18	5.78	8.33	3.55	1.18	0.52	2.25	99.02
NT-2/10	B	48.15	1.58	16.63	10.17	0.17	7.59	8.78	3.06	0.61	0.45	1.88	99.07
NT-20/1*	BA	51.10	1.54	16.59	9.52	0.12	4.42	7.71	3.24	1.39	0.32	2.74	98.69
NT-20/15	TA	59.39	0.96	16.36	6.39	0.10	2.54	5.21	4.04	2.61	0.27	1.18	99.04
NT-20/26**	TA	59.00	1.01	17.34	6.24	0.17	2.34	5.53	4.48	1.87	0.48	0.65	99.10
NT-20/27**	B	47.83	1.26	18.65	9.05	0.14	5.95	9.49	3.10	1.09	0.27	2.11	98.94
NT-20/28**	BA	50.95	1.13	15.77	8.92	0.16	8.24	7.90	2.63	1.73	0.38	1.12	98.94
NT-20/30	BTA	50.30	1.86	16.35	10.96	0.17	3.77	7.89	4.23	0.67	0.46	1.82	98.49
NT-20/31	BTA	50.27	1.84	16.22	11.09	0.15	3.81	7.12	4.25	1.35	0.44	2.03	98.57
NT-20/34	A	58.74	0.84	16.92	6.90	0.12	2.73	6.81	3.34	1.86	0.21	0.63	99.11
NT-20/35	A	58.24	0.85	17.30	6.55	0.13	2.99	6.58	3.41	1.68	0.22	1.20	99.16
NT-20/36	A	58.08	0.85	17.16	6.59	0.12	3.01	6.60	3.29	1.86	0.22	1.39	99.17

Table 1. (Contd.)

Sample no.	Rock	SiO_2	TiO_2	Al_2O_3	FeO	MnO	MgO	CaO	Na_2O	K_2O	P_2O_5	LOI	Total
NT-20/37	A	58.00	0.86	17.27	6.71	0.11	2.71	6.34	3.48	2.08	0.21	1.25	99.02
NT-20/38	BA	54.39	0.89	17.15	7.32	0.10	5.77	7.49	3.43	1.09	0.19	1.14	98.95
NT-22/1	A	57.13	1.07	17.32	7.50	0.14	2.68	5.99	3.36	1.85	0.29	1.74	99.05
NT-24/4**	B	49.07	1.18	17.86	9.05	0.16	6.22	8.55	3.00	1.26	0.38	2.25	98.97
NT-24/5**	A	61.31	1.06	16.43	5.59	0.09	1.92	4.98	3.92	2.29	0.25	1.56	99.40
NT-24/9	BTA	50.17	2.54	15.56	12.31	0.22	2.77	7.62	4.17	1.29	1.00	1.20	98.85
NT-24/13	BA	50.86	1.47	17.16	8.79	0.16	5.39	9.03	3.47	0.63	0.48	1.65	99.09
NT-24/16	TB	47.80	2.45	15.56	12.50	0.23	3.84	8.25	4.16	1.40	0.72	1.90	98.81
NT-24/17	TB	49.47	2.14	16.45	11.93	0.19	2.94	7.75	3.86	1.41	0.65	1.93	98.72
NT-24/18	BTA	51.61	1.56	16.89	9.75	0.20	3.98	8.02	3.89	1.45	0.76	0.82	98.92
N-4135/17	BTA	50.17	1.90	16.63	9.69	0.26	4.26	7.20	4.69	1.86	0.45	2.38	99.49
N-4135/19	BA	52.57	2.15	15.86	11.55	0.26	3.04	6.97	4.42	0.71	0.60	0.37	98.50
N-4135/20	TB	50.17	2.70	15.56	10.40	0.11	4.46	8.25	3.73	1.29	0.62	1.68	98.97
NT-22/23***	B	50.05	1.21	17.83	9.32	0.14	4.59	10.05	3.43	1.12	0.23	0.88	98.85
NT-22/24***	TB	48.98	1.31	20.35	9.23	0.11	3.13	8.71	3.51	2.06	0.26	1.26	98.93
NT-22/25***	BTA	54.58	1.24	17.48	7.64	0.13	3.50	6.54	5.74	0.98	0.37	0.88	99.08
NT-24/6***	TA	55.01	0.96	16.77	6.85	0.18	4.17	7.12	4.85	1.93	0.52	0.85	99.20
NT-24/7***	TA	54.28	0.97	17.03	6.72	0.19	3.88	7.20	4.08	3.03	0.54	1.00	98.93
NT-24/8***	BTA	54.29	1.00	17.14	8.13	0.36	3.50	6.49	4.94	1.75	0.56	0.95	99.10
NT-24/15***	BTA	53.29	0.99	16.77	8.21	0.24	4.04	6.04	5.14	2.45	0.81	1.14	99.13
NT-22/26***	R	74.75	0.22	12.72	1.96	0.06	0.34	1.45	3.12	3.49	0.05	1.35	99.51
NT-22/27***	R	69.28	0.64	14.40	2.98	0.11	0.65	2.27	5.64	2.31	0.13	1.06	99.47
NT-20/21	Gr	75.57	0.17	12.69	1.74	0.05	0.44	0.88	3.76	3.91	0.04	0.45	99.70

Note: FeO is total iron. Rock abbreviations: **B**, basalt; **TB**, trachybasalt; **BA**, basaltic andesite; **BTA**, basaltic trachyandesite; **A**, andesite; **TA**, trachyandesite; **R**, rhyolite; and **Gr**, biotite granite.
* Rock of the vent facies.
** Dike.
*** Rock of the ACM complex.

bimodal association, into the fields of basalt, trachybasalt, basaltic trachyandesite, and trachyandesite. The concentrations of major elements in the rocks of the two associations (rift-related and ACM) show only minor differences (Fig. 4). It can be noted that the basalts and trachybasalts of ACM are in general poorer in TiO_2, MgO, FeO, and P_2O_5 and richer in Al_2O_3. Compared with the silica-rich rift-related rocks, the basaltic trachyandesites and trachyandesites of ACM have similarly low TiO_2 and MgO and higher P_2O_5 and Na_2O concentrations.

Trace Elements

The primitive-mantle normalized (Sun and McDonough, 1989) concentrations of trace elements in the basic rocks of the bimodal association of the Noen and Tost ranges (Table 2) are presented in spider diagrams (Fig. 5). The concentrations of incompatible trace elements in the rocks of the rift-related complex show considerable variations independent of SiO_2 content. Some features of the trace element distribution patterns are typical of all basic constituents of bimodal associations. Rocks with the lowest SiO_2 contents (basalts and trachybasalts) show distinct negative Ta–Nb anomalies (Fig. 5a) [$(La/Nb)_{PM} = 1.7–2.6$], a slight negative anomaly in Ti, and positive anomalies for K and Pb. The REE distribution patterns of the rift-related basalts and trachybasalts of the Noen and Tost ranges (Fig. 5b) show moderate enrichment in light rare earth elements (LREE) relative to heavy REE (HREE), $(La/Yb)_{PM} = 3.28–4.96$.

More silica-rich basaltoid varieties of the bimodal association (basaltic andesites and basaltic trachyandesites, andesites, and trachyandesites) are similar to the basalts and trachybasalts in trace-element distribution patterns (Figs. 5c, 5e) and concentration levels. A somewhat more pronounced negative anomaly in Ta and Nb was observed in the basaltic andesites, basaltic trachyandesites [$(La/Nb)_{PM} = 2.1–3.5$], andesites, and trachyandesites [$(La/Nb)_{PM} = 1.6–4.0$]. The REE

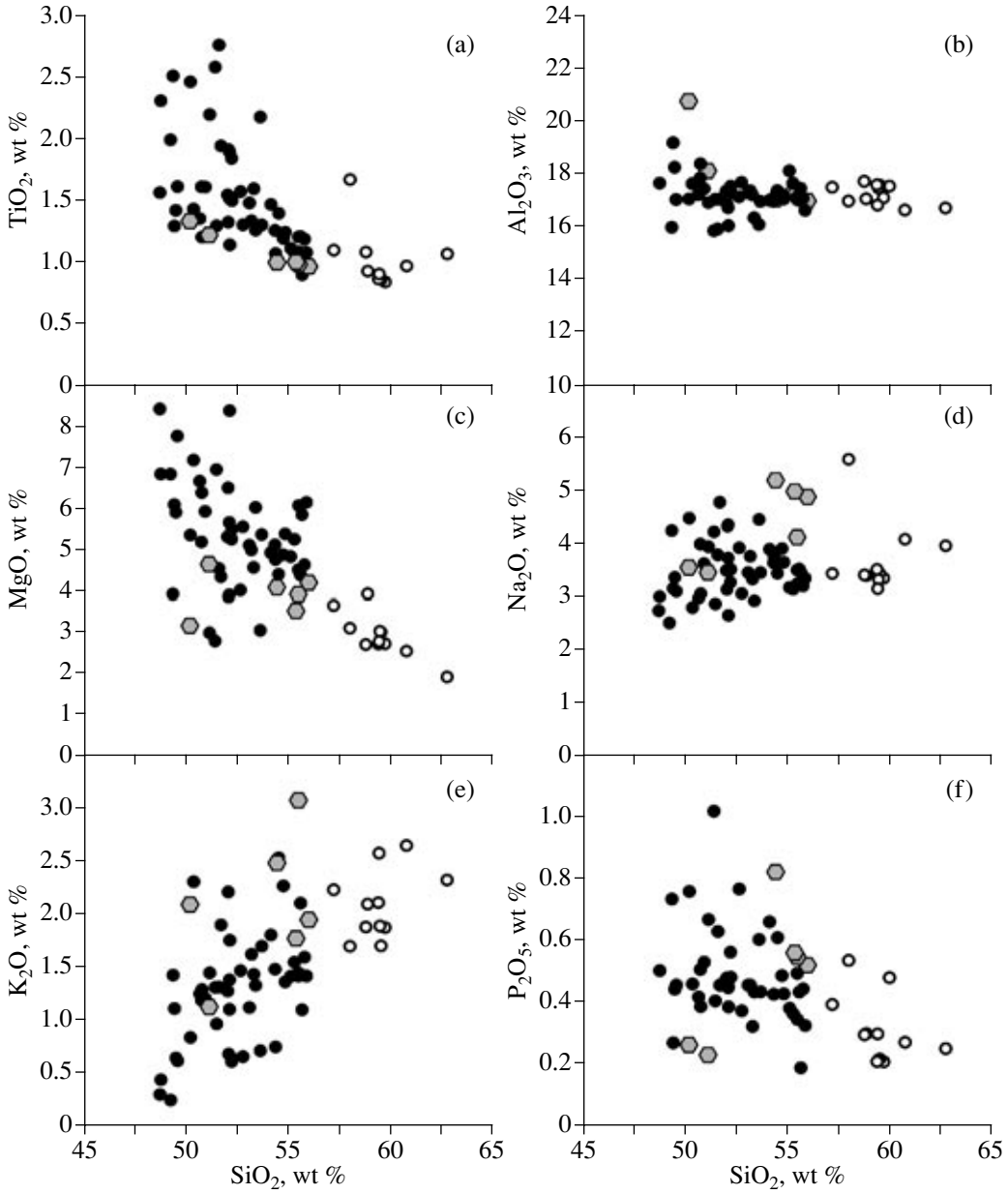

Fig. 4. Variations in selected major elements as functions of SiO_2 in the basic rocks of the rift-related bimodal association of the Noen and Tost ranges and the ACM complex. Symbols are the same as in Fig. 3.

distribution patterns of the basaltic andesites, basaltic trachyandesites (Fig. 5d), andesites, and trachyandesites (Fig. 5f) are somewhat different from those of the basalts and trachybasalts, primarily in the degree of LREE enrichment relative to HREE. For instance, most rift-related basaltic andesites and basaltic trachyandesites have $(La/Yb)_{PM}$ values from 3.23 to 6.93, which are somewhat higher than those of the basalts and trachybasalts. Conspicuous among these rocks are strongly LREE enriched compositions with $(La/Yb)_{PM}$ ratios as high as 8.32 (sample NT-1/24) and 13.17 (sample NT-1/23). The andesites and trachyandesites also show an LREE enrichment relative to HREE, $(La/Yb)_{PM}$ = 3.97–9.20.

A comparison of the trace-element distribution patterns of basaltoids from the rift-related and ACM associations showed that the rocks with the lowest SiO_2 contents (basalts and trachybasalts) are in general similar (Fig. 5a): there are a pronounced negative Ta–Nb anomaly [$(La/Nb)_{PM}$ = 2.2] and relative enrichment in K and Pb. However, compared with the rift-related basaltoids, the ACM basalts and trachybasalts are depleted in Nb, Ta, Y, and REE and enriched in Ba, U, Th, and K; in addition, they show a negative Zr–Hf anomaly and a lower degree of LREE enrichment rela-

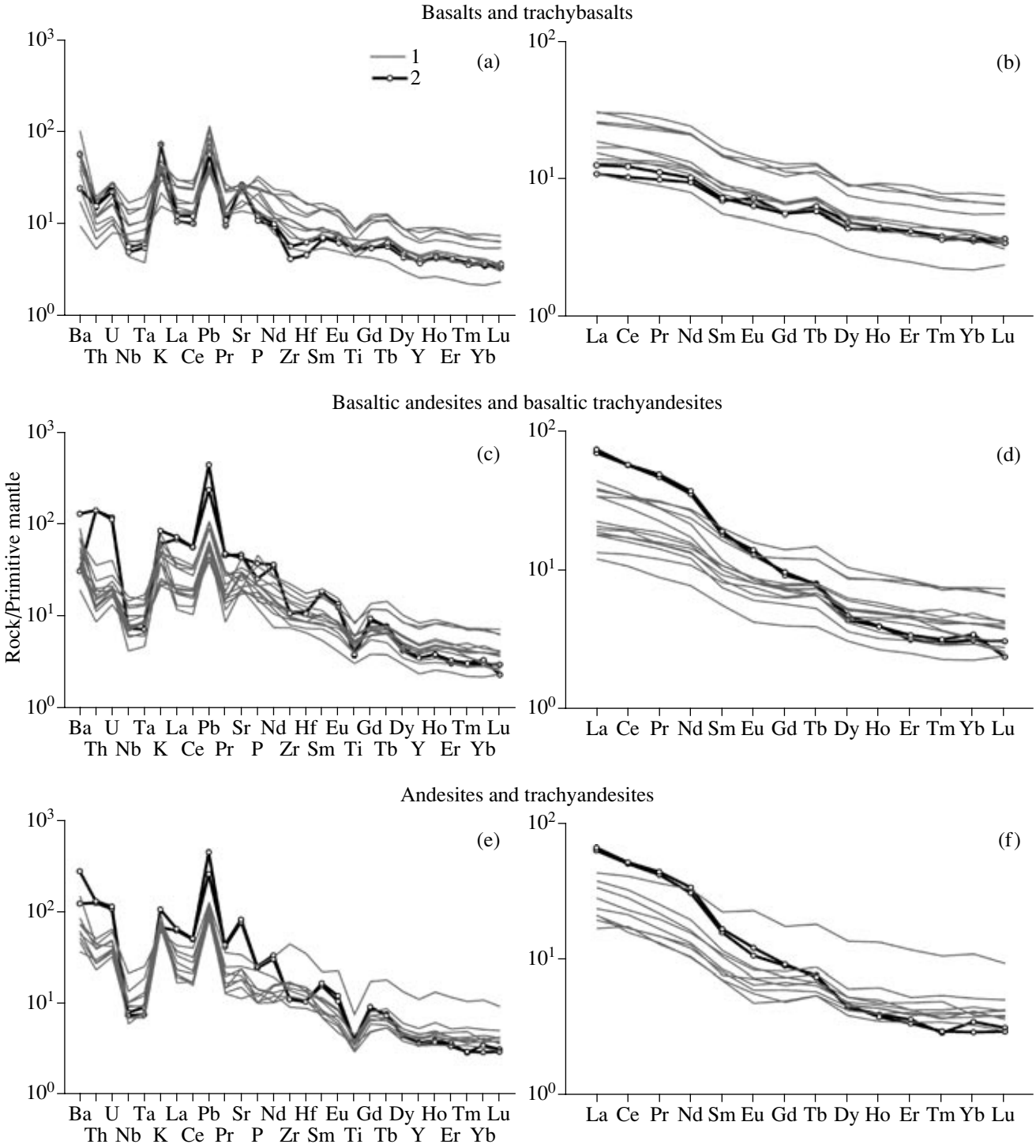

Fig. 5. Primitive mantle normalized (Sun and McDonough, 1989) distribution patterns of trace and rare earth elements for the basic rocks of the bimodal association of the Noen and Tost ranges and the ACM complex. (1) Rocks of the bimodal association and (2) rocks of the ACM complex.

tive to HREE, $(La/Yb)_{PM}$ = 3.03–3.41 (Fig. 5b). More significant differences were established between the compositions of the basaltic trachyandesites and trachybasalts of the ACM complex and the same rocks of the rift-related bimodal association (Fig. 5c, 5e). The former are strongly enriched in Ba, Th, U, and Pb and show a more pronounced negative Nb and Ta anomaly [$(La/Nb)_{PM}$ = 7.9–9.8] and a distinct negative anomaly for Zr and Hf. Moreover, they have strongly fractionated REE distribution patterns with $(La/Yb)_{PM}$ = 18.1–22.6.

Table 2. Concentrations of trace elements (ppm) in the basic rocks of the bimodal association of the Noen and Tost ranges and the ACM complex

Element	NT-1/1	NT-1/3	NT-1/9	NT-1/12	NT-1/23	NT-1/24	NT-2/1	NT-2/2	NT-2/3	NT-2/5	NT-2/8	NT-2/10	NT-20/1*	NT-20/15
	B	TB	TB	BA	BTA	BTA	BA	TA	TB	A	B	B	BA	TA
Li	26	29	26	26	22	21	16	25	33	11	25	12	17	11
Be	1.6	0.97	1.6	1.2	1.3	1.3	1.1	2.5	1.4	1.2	1.6	0.93	0.92	1.6
Sc	18	27	24	18	11	12	23	21	29	7.6	26	15	17	6.9
Ti	9083	5882	7515	7131	6546	6121	8524	10047	11770	4567	9103	7229	6966	4780
V	127	157	154	136	131	105	160	124	233	154	212	133	173	112
Cr	119	244	105	95	68	49	165	24	29	39	138	165	26	36
Co	30	27	27	28	22	20	30	14	26	18	36	35	25	13
Ni	67	99	62	61	48	38	87	4.2	13	29	68	98	5.0	23
Cu	33	41	45	23	67	29	23	7.7	35	58	48	44	15	11
Zn	62	55	65	83	104	92	106	112	96	71	90	84	89	51
Ga	12	12	15	15	16	16	16	22	22	15	21	14	16	15
Rb	1.6	34	9.9	9.2	16	20	4.1	15	6.3	22	14	5.7	12	34
Sr	316	411	595	630	771	658	424	768	611	402	618	352	455	254
Y	21	19	22	21	16	21	24	53	30	20	33	21	19	17
Zr	135	86	133	137	177	168	137	531	164	174	249	113	111	192
Nb	5.9	5.1	7.3	6.8	12	7.7	5.6	16	7.5	6.9	13	4.6	4.5	7.8
Cs	1.3	1.2	0.72	0.53	0.21	0.67	0.63	0.43	0.70	0.16	0.47	9.0	0.71	0.99
Ba	72	464	479	286	537	675	144	1112	777	457	361	131	335	273
La	9.7	11	14	14	29	25	13	32	19	17	23	10	9.9	12
Ce	25	27	33	33	65	55	33	79	48	41	53	27	25	34
Pr	3.6	3.5	4.4	4.4	7.9	6.4	4.5	10	6.7	4.7	6.9	3.8	3.4	3.7
Nd	17	16	19	19	31	25	21	47	30	19	31	17	16	15
Sm	4.0	3.6	4.2	4.3	5.5	4.7	5.0	10	7.0	3.9	6.8	4.4	3.8	3.3
Eu	1.3	1.2	1.4	1.4	1.5	1.4	1.5	4.0	2.4	1.1	2.1	1.3	1.3	0.84
Gd	4.2	3.6	4.2	4.4	4.6	4.5	4.9	11	7.0	4.2	6.5	4.2	4.0	3.1
Tb	0.69	0.61	0.73	0.73	0.66	0.73	0.80	1.8	1.1	0.64	1.1	0.72	0.68	0.54
Dy	4.1	3.5	4.2	4.1	3.2	4.0	4.9	10	5.9	3.8	7.1	4.2	3.9	3.3
Ho	0.84	0.71	0.89	0.85	0.61	0.81	0.98	2.3	1.2	0.79	1.4	0.84	0.84	0.68
Er	2.3	2.1	2.4	2.3	1.6	2.4	2.6	5.9	3.3	2.2	4.0	2.3	2.2	2.1
Tm	0.36	0.30	0.36	0.36	0.24	0.34	0.37	0.86	0.48	0.30	0.60	0.36	0.33	0.30
Yb	2.0	1.9	2.1	2.1	1.5	2.1	2.5	5.5	2.8	1.9	3.5	2.2	2.1	2.1
Lu	0.28	0.25	0.30	0.33	0.21	0.31	0.34	0.76	0.45	0.32	0.54	0.29	0.31	0.30
Hf	3.0	2.2	2.9	3.3	4.2	3.7	3.3	12	4.0	4.4	5.6	2.8	2.9	4.9
Ta	0.38	0.27	0.47	0.44	0.66	0.45	0.36	1.1	0.47	0.41	0.86	0.25	0.29	0.57
Pb	2.9	3.1	4.8	3.2	7.8	6.6	4.1	9.1	8.5	7.1	5.4	2.6	4.5	8.0
Th	0.51	1.2	1.1	1.1	2.3	1.4	0.83	4.1	1.7	2.6	1.9	0.65	1.2	2.8
U	0.18	0.38	0.37	0.37	0.64	0.44	0.31	1.36	0.54	0.86	0.65	0.23	0.40	0.88

Table 2. (Contd.)

Element	NT-20/26**	NT-20/27	NT-20/28	NT-20/30	NT-20/31	NT-20/34	NT-20/36	NT-20/37	NT-20/38	NT-22/1	NT-24/4**	NT-24/5**	NT-24/9	NT-24/13
	TA	B	BA	BTA	BTA	A	A	A	BA	A	B	A	BTA	BA
Li	5.8	28	30	18	25	7.8	12	14	7.1	16	43	34	12	13
Be	1.6	0.76	0.87	1.2	1.7	1.1	1.1	1.5	0.83	1.5	1.4	2.2	2.3	1.0
Sc	11	14	13	18	38	14	17	23	9.0	21	25	14	28	24
Ti	4880	6019	5324	8200	11694	3889	4134	5101	4148	6008	6579	5944	11155	7367
V	138	166	116	233	351	170	165	180	176	196	183	129	168	194
Cr	0.10	99	158	0.1	3.0	26	25	25	172	7.9	81	4.8	2.5	64
Co	8.9	31	34	26	36	16	17	23	25	15	36	16	24	31
Ni	0.50	53	124	0.5	5.0	16	17	21	108	3.9	68	5.6	0.08	51
Cu	4.7	46	39	30	27	38	48	35	27	7.9	43	27	9.2	38
Zn	100	93	88	104	108	64	66	90	58	82	113	63	127	79
Ga	17	16	14	18	24	15	16	20	15	19	18	18	21	19
Rb	27	19	39	3.7	18	29	34	45	11	47	36	48	16	5.1
Sr	571	584	399	481	697	338	412	537	451	538	572	449	444	983
Y	21	13	15	23	36	16	19	25	12	22	19	22	41	20
Zr	163	65.5	96.8	138	206	141	141	197	90	108	99	203	269	120
Nb	7.1	3.4	4.8	6.1	9.4	5.2	5.2	7.7	3.2	4.5	4.8	10	11	5.8
Cs	0.41	0.85	3.0	0.06	0.15	0.44	0.69	1.3	0.17	1.9	0.28	0.22	0.08	1.2
Ba	539	187	242	274	495	350	389	634	262	424	290	550	385	281
La	28	8.1	13	15	33	16	16	21	9.0	14	13	25	25	17
Ce	62	19	31	38	70	30	33	44	21	33	33	54	64	39
Pr	7.2	2.5	4.1	5.0	8.0	3.7	4.2	5.6	2.5	4.2	4.2	6.1	8.8	5.4
Nd	28	11	17	22	34	15	17	22	11	18	17	23	40	23
Sm	5.4	2.6	3.5	4.7	7.6	3.3	3.8	5.1	2.6	3.6	3.9	4.9	9.4	5.1
Eu	1.5	0.89	1.1	1.4	2.2	0.98	1.0	1.5	0.74	1.3	1.4	1.3	2.8	1.6
Gd	4.6	2.7	3.5	4.8	7.5	3.0	3.7	5.0	2.5	4.0	4.0	4.5	8.7	4.4
Tb	0.67	0.39	0.53	0.77	1.2	0.54	0.58	0.87	0.39	0.68	0.71	0.77	1.5	0.65
Dy	3.6	2.4	2.8	4.7	6.8	3.0	3.5	4.7	2.4	4.1	3.8	4.1	8.1	3.6
Ho	0.74	0.46	0.55	0.93	1.4	0.60	0.75	1.1	0.45	0.81	0.78	0.85	1.6	0.76
Er	2.0	1.3	1.6	2.5	4.0	1.7	2.0	2.7	1.3	2.4	2.0	2.1	4.3	2.3
Tm	0.32	0.18	0.23	0.42	0.61	0.28	0.33	0.44	0.18	0.40	0.31	0.35	0.61	0.30
Yb	2.1	1.1	1.5	2.3	3.6	1.7	2.0	2.6	1.1	2.0	2.0	2.3	3.8	1.6
Lu	0.34	0.19	0.23	0.35	0.54	0.24	0.35	0.41	0.20	0.31	0.27	0.34	0.60	0.25
Hf	3.9	1.7	2.5	3.3	4.6	3.6	3.6	4.9	2.2	2.9	2.0	4.5	5.9	2.9
Ta	0.39	0.17	0.27	0.36	0.57	0.30	0.33	0.52	0.21	0.35	0.30	0.81	0.75	0.39
Pb	7.7	8.0	2.9	4.3	6.6	6.6	6.1	7.7	3.9	8.8	3.1	8.7	7.5	4.7
Th	4.2	0.79	1.2	1.9	3.4	2.2	2.6	3.7	1.3	3.8	0.94	4.8	1.2	1.5
U	0.95	0.25	0.40	0.49	0.92	0.73	0.81	1.1	0.44	1.1	0.27	1.5	0.46	0.47

Table 2. (Contd.)

Element	NT-24/16	NT-24/17	NT-24/18	NT-22/23**	NT-22/24**	NT-22/25**	NT-24/15***	NT-24/6***	NT-24/7***	NT-24/8***	NT-22/26***	NT-22/27***	NT-20/21
	TB	TB	BTA	B	TB	BTA	BTA	TA	TA	BTA	R	R	Gr
Li	19	22	10	14	37	44	21	16	15	32	9.0	16	25
Be	2.3	2.1	1.6	1.1	0.88	1.5	1.5	2.2	2.0	2.5	2.6	4.3	1.9
Sc	32	24	28	34	21	15	15	14	15	15	8.0	16	0.83
Ti	11828	11034	8035	7064	7444	6652	5222	5139	5195	5072	1734	5120	1042
V	284	254	215	249	248	157	180	170	158	162	17	37	5.9
Cr	1.86	53	33	217	42	38	12	18	15	14	22	33	4.9
Co	30	38	27	36	22	21	30	28	17	8.4	2.0	3.5	1.5
Ni	5.0	56	30	62	20	20	23	23	25	24	8.3	10	0.5
Cu	14	21	30	5.9	7.4	40	20	13	44	2.0	6.3	5.9	5.0
Zn	122	111	107	49	40	65	107	119	72	163	29	53	15
Ga	23	21	18	20	20	19	19	19	19	18	15	20	12
Rb	17	22	14	26	49	8.3	70	44	69	64	80	38	88
Sr	487	552	552	606	573	553	986	1752	1866	1065	139	162	95.0
Y	40	44	38	19	18	15	17	18	17	17	20	24	11
Zr	269	194	241	50	69	120	130	134	130	133	64	168	71
Nb	11	9.8	10.0	3.8	4.3	6.0	5.7	6.0	5.6	5.9	5.7	6.2	7.4
Cs	0.08	0.05	0.86	1.5	3.5	0.85	0.57	0.47	0.26	0.47	3.0	0.40	1.7
Ba	425	324	510	183	429	271	976	916	2072	232	516	469	825
La	23	19	28	8.1	9.4	12	55	47	49	52	16	17	23
Ce	58	46	66	20	24	30	112	97	100	111	32	34	42
Pr	7.9	6.4	9.0	2.8	3.2	3.5	14	12	12	13	3.7	4.5	4.0
Nd	35	30	39	14	15	15	53	44	48	51	13	18	13
Sm	8.0	7.0	8.2	3.3	3.4	3.3	8.9	7.3	7.8	8.5	3.0	3.9	2.2
Eu	2.5	2.1	2.2	1.3	1.1	0.98	2.2	1.9	2.1	2.4	0.50	1.1	0.41
Gd	8.0	7.4	7.6	3.5	3.5	3.0	6.0	5.5	5.7	5.7	2.6	3.7	2.2
Tb	1.3	1.3	1.2	0.58	0.63	0.56	0.78	0.76	0.73	0.80	0.48	0.60	0.31
Dy	7.0	6.9	6.7	3.4	3.8	3.2	3.4	3.4	3.5	3.6	2.8	3.5	2.0
Ho	1.5	1.6	1.5	0.73	0.77	0.62	0.67	0.67	0.64	0.67	0.65	0.76	0.38
Er	4.0	4.5	4.2	2.1	2.1	1.8	1.7	1.8	1.7	1.6	1.9	2.3	1.2
Tm	0.57	0.64	0.59	0.32	0.30	0.24	0.26	0.24	0.24	0.25	0.31	0.41	0.22
Yb	3.5	4.0	3.8	1.8	1.9	1.7	1.7	1.8	1.5	1.6	2.2	2.6	1.4
Lu	0.53	0.62	0.52	0.28	0.30	0.23	0.19	0.26	0.24	0.25	0.35	0.34	0.25
Hf	5.4	4.3	5.2	1.5	2.1	3.3	3.5	3.4	3.4	3.7	2.1	4.1	2.6
Ta	0.66	0.67	0.59	0.24	0.26	0.36	0.32	0.39	0.32	0.37	0.43	0.36	0.67
Pb	5.4	6.3	7.8	4.4	4.1	6.0	17	32	19	32	9.2	9.5	18
Th	1.2	1.8	1.6	1.5	1.5	1.6	13	12	12	13	7.1	4.1	12
U	0.45	0.63	0.55	0.60	0.51	0.51	2.6	2.4	2.6	2.7	1.4	1.1	1.2

Note: Rock abbreviations: **B**, basalt; **TB**, trachybasalt; **BA**, basaltic andesite; **BTA**, basaltic trachyandesite; **A**, andesite; **TA**, trachyandesite; **R**, rhyolite; and **Gr**, biotite granite.
* Rock of the vent facies.
** Dike.
*** Rock of the ACM complex.

Table 3. Rb–Sr, Sm–Nd, and O isotope data for the basic rocks of the bimodal association of the Noen and Tost ranges and the ACM complex

Sample no.	Rock	Rb, ppm	Sr, ppm	$^{87}Rb/^{86}Sr$	$^{87}Sr/^{86}Sr$	±2σ	$(^{87}Sr/^{86}Sr)_0$
NT-1/9	TB	10.8	718.9	0.0435	0.70397	14	0.70377
NT-1/23	BTA	20.4	980	0.0602	0.70446	14	0.70418
NT-2/3	TB	6.6	666.2	0.0287	0.70402	16	0.70389
NT-2/8	B	15.5	552.5	0.0811	0.70415	15	0.70378
NT-2/10	B	8.9	470.8	0.0547	0.70385	11	0.70360
NT-20/1*	BA	18	571	0.0914	0.70416	16	0.70374
NT-20/15	TA	68.8	428	0.4649	0.70593	18	0.70383
NT-20/26**	TA	32.2	679	0.1372	0.70489	14	0.70427
NT-20/28**	BA	58.3	544	0.3101	0.70545	15	0.70404
NT-20/36	A	37.8	475	0.23	0.70520	14	0.70416
NT-22/23***	B	27	601	0.1288	0.70484	18	0.70426
NT-22/24***	TB	70.2	656	0.3094	0.70556	18	0.70416
NT-20/21	Gr	95.1	90	3.062	0.71807	11	0.70421
Sample no.	Sm, ppm	Nd, ppm	$^{147}Sm/^{144}Nd$	$^{143}Nd/^{144}Nd$	±2σ	$\varepsilon_{Nd}(T)$	$\delta^{18}O_{SMOW}$
NT-1/9	5.32	23.23	0.1384	0.512838	7	6.27	5.2
NT-1/23	6.97	38.87	0.1074	0.512678	5	4.41	7.2
NT-2/3	7.20	31.13	0.1398	0.512828	8	6.02	5.4
NT-2/8	5.94	26.39	0.1361	0.512821	7	6.04	6.1
NT-2/10	5.09	21.05	0.1461	0.512874	8	6.66	4.5
NT-20/1*	4.52	18.33	0.1476	0.512823	8	5.61	0.3
NT-20/15	5.92	27.86	0.1273	0.512775	7	5.50	7.1
NT-20/26**	6.69	34.27	0.1170	0.512696	6	4.37	6.3
NT-20/28**	4.73	21.95	0.1292	0.512750	9	4.93	4.5
NT-20/36	4.16	18.88	0.1319	0.512759	7	4.99	8
NT-22/23***	3.47	13.81	0.1521	0.512840	8	5.76	–2.4
NT-22/24***	3.74	15.61	0.1449	0.512763	7	4.54	–1.5
NT-20/21	2.22	13.16	0.1009	0.512678	7	4.68	9.3

Note: Rock abbreviations: **B**, basalt; **TB**, trachybasalt; **BA**, basaltic andesite; **BTA**, basaltic trachyandesite; **A**, andesite; **TA**, trachyandesite; and **Gr**, biotite granite. The $(^{87}Sr/^{86}Sr)_0$ and $\varepsilon_{Nd}(T)$ values were calculated for an age of 318 Ma.
* Rock of the vent facies.
** Dike.
*** Rock of the ACM complex.

Sr–Nd–O ISOTOPIC SYSTEMATICS

The isotopic data for the basic rocks of the bimodal association of the Noen and Tost ranges are shown in Table 3 and Fig. 6. Initial Sr isotope ratios and $\varepsilon_{Nd}(T)$ values were calculated for an age of 318 Ma (Kozlovsky et al., 2005). As can be seen from Fig. 6a, the basic rocks of the bimodal association form a linear trend near the field of compositions depleted in radiogenic strontium and enriched in radiogenic neodymium; the most depleted compositions are characteristic of the basalts and trachybasalts: $\varepsilon_{Nd}(T) = 6.0–6.7$ and $(^{87}Sr/^{86}Sr)_0 = 0.70360–0.70389$. The SiO_2 richer basaltic andesites, basaltic trachyandesites, andesites, and trachyandesites plot into the field of less depleted compositions with $\varepsilon_{Nd}(T) = 4.4–5.6$ and $(^{87}Sr/^{86}Sr)_0 = 0.70374–0.70427$.

With respect to oxygen isotopes, compositions with $\delta^{18}O$ values between 4.5 and 8‰ are dominant within the whole range of volcanic rocks from the bimodal association of the Noen and Tost ranges (Fig. 6b); the isotopic ratios of the basalts and trachybasalts are most similar to those of mantle melts, $\delta^{18}O = 4.5–6.1‰$ (Pokrovskii, 2000). An exception is sample NT-20/1 of vent-facies basaltic andesite showing a low $\delta^{18}O$ value of 0.3‰, which is probably related to secondary alteration by heated meteoric waters near the volcanic crater.

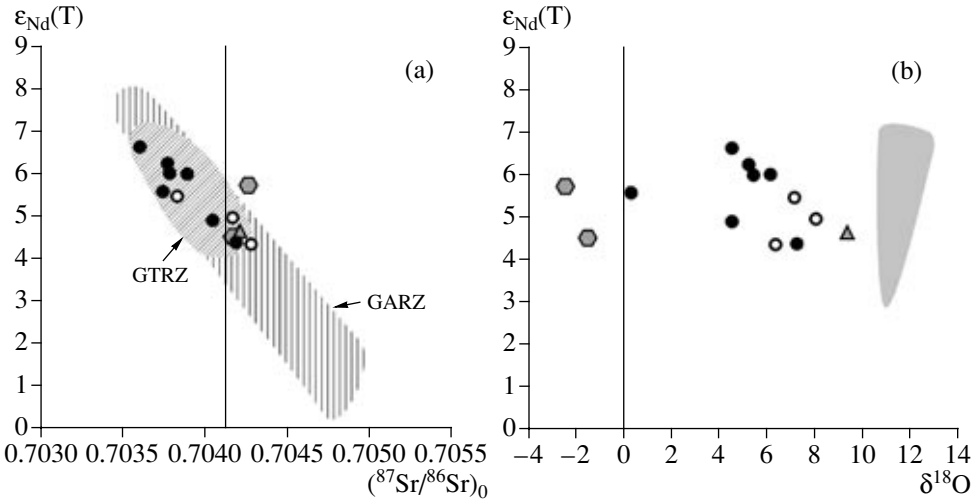

Fig. 6. Diagrams of the Sr, Nd, and O isotopic compositions of the basic rocks of the bimodal association of the Noen and Tost ranges and the ACM complex. Also shown for comparison are the fields of the isotopic compositions of basaltoids of the bimodal associations of the Gobi–Altai rift zone (GARZ) (Yarmolyuk et al., 1999; our unpublished data) and the Gobi–Tien Shan rift zone (GTRZ), including the associations of the framing of the Haan Bogd peralkaline granite massif in the eastern GTRZ (Yarmolyuk et al., 1999; our unpublished data) and the Noen and Tost ranges. The shaded field shows the compositions of rocks from the ophiolite and island-arc complexes of the Hercynian basement (our unpublished data). Other symbols are the same as in Fig. 3.

For the sake of comparison, basic rocks from the ACM volcanic belt were also studied. Their Sr [$(^{87}Sr/^{86}Sr)_0$ of 0.70416 and 0.70426] and Nd isotopic characteristics [$\varepsilon_{Nd}(T)$ of 4.5 and 5.8] fall within the range of rift-related rocks, primarily silica-rich basaltic trachyandesites and andesites. More significant differences were observed between the basic rocks of ACM and rift-related complexes in oxygen isotope ratios. The basic rocks of ACM are depleted in ^{18}O and show negative $\delta^{18}O$ values between –1.5 and –2.4‰; however, these rocks underwent greenstone alterations, and their low $\delta^{18}O$ values cannot be considered as reflecting the oxygen isotope composition of ACM magmas. Nonetheless, these results allow us to suppose different conditions for the continental margin and rift-related magmatism.

PETROGENETIC MODELS FOR THE BASIC ROCKS

Variations in the concentration of major and trace elements and isotopic ratios of basic rocks have traditionally been attributed to crystallization differentiation, contamination, changes in the degree of melting and heterogeneity of the source material, and combinations of these processes. However, the determination of which phenomenon was responsible for particular variations in rock composition may be difficult or impossible.

Crystallization Differentiation

Rocks with MgO contents below 8% are most common among the rift-related basic rocks of the bimodal association of the Noen and Tost ranges, i.e., they cannot be regarded as primary melts from mantle peridotites equilibrated with olivine Fo_{89} (Palme and O'Neill, 2003; Klein, 2003). The existence of a continuous array from basalts and trachybasalts to andesites and trachyandesites is in agreement with variations in mineral composition: the fraction of olivine phenocrysts decreases and that of clinopyroxene and plagioclase increases in this direction. This is compelling evidence for the fractional crystallization of the basic melts of the bimodal association of the Noen and Tost ranges. The concentration of MgO is the most sensitive indicator of the fractionation of such melts. The concentrations of the compatible trace elements Ni, Co, and Cr decrease with decreasing MgO (Fig. 7). In the basaltoids with MgO > 4.5%, Ni content falls from 124 to 5 ppm (Fig. 7a), and that of Cr, from 244 to 26 ppm. The less magnesian rocks (mainly andesites and trachyandesites) show low Ni (0.5–56 ppm) and Cr concentrations (0.1–53 ppm) and no significant correlations. In contrast to Ni and Cr, the concentration of Co decreases monotonously from 36 to 9 ppm with decreasing MgO content within the whole range of rift-related basic rocks (Fig. 7b). Such trends are controlled by the fractionation of olivine, which is the main repository of Ni in the most magnesian rocks, and pyroxene, which is the major host for Co within the whole compositional range of basic rocks. The fractionation of plagioclase is reflected in Sr variations. The concentration of Sr increases from 316 to 771 ppm with decreasing MgO in the rocks with MgO > 4.5% (Fig. 7c). The less magnesian rocks show a decrease in Sr concentration to 254 ppm. Thus, the Sr concentration passes through a maximum at MgO ≈ 4.5%, which probably marks the

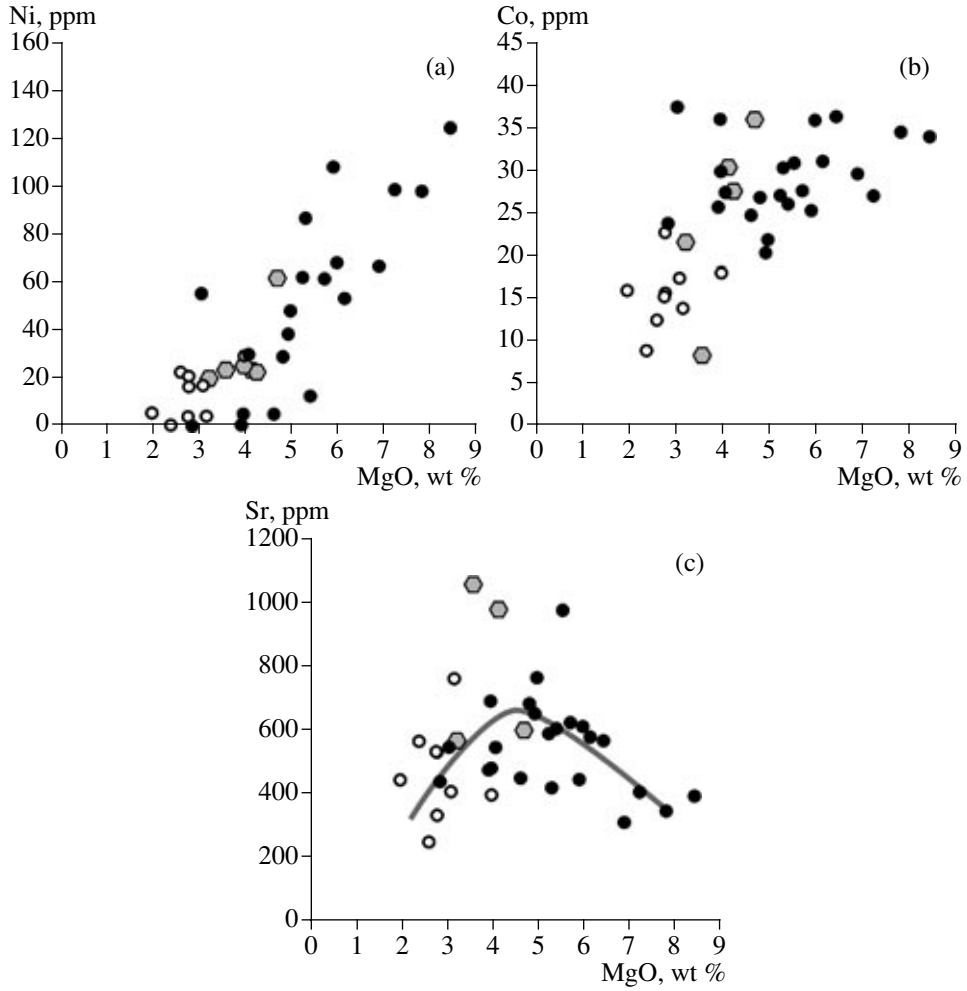

Fig. 7. Variations in compatible element concentrations (Ni, Cr, and Co) as functions of MgO content in the basic rocks of the bimodal association of the Noen and Tost ranges and the ACM complex. Figure 7c shows the trend of Sr concentration indicating that extensive plagioclase fractionation began in melts with MgO < 4.5%. Symbols are the same as in Fig. 3.

beginning of extensive plagioclase fractionation. In general, the analysis of the behavior of compatible trace elements suggested that the rift-related basaltoids and andesites were affected by the sequential fractional crystallization of olivine, pyroxene, and plagioclase.

Within the whole compositional range from basaltoid to andesite, the incompatible trace elements, such as REE, Y, Zr, Nb, and Hf, show no significant negative correlations with MgO, which are typical of the products of crystal fractionation (Figs. 8a, 8c, 8d). The concentrations of these elements are rather scattered, and the ranges observed in rocks with different MgO contents completely overlap. The concentrations of Ta, Pb, U, and Th increase with decreasing MgO content (Fig. 8b). This tendency is most distinct in the andesites and trachyandesites with MgO < 4%, although they also display a considerable scatter in composition.

The proportions of incompatible trace elements in the rift-related basaltoids vary considerably and independently of MgO content (Figs. 8e, 8f). Regular changes were associated only with the transition to andesites, when the Nb/U, Nb/Th, and Nb/Ta ratios decreased, and La/Sm, Th/Ta, Th/Y, Th/La, and K/Ti increased (Figs. 8e, 8f). On the other hand, the rift-related basaltoids and andesites of the Noen and Tost ranges do not usually show positive linear correlations between the concentrations of incompatible elements (e.g., Nb–Y, Zr–Y, La–Yb, Nb–La), which are characteristic of the differentiation products of a homogeneous melt. Thus, based on the behavior of incompatible elements, it can be concluded that the compositions of most rift-related basaltoids and andesites of the bimodal association of the Noen and Tost ranges were only slightly affected by crystallization differentiation, and their variations were controlled by other factors.

Sources of Rift-Related Basic Rocks

The rift-related basic rocks of the bimodal association of the Noen and Tost ranges show many character-

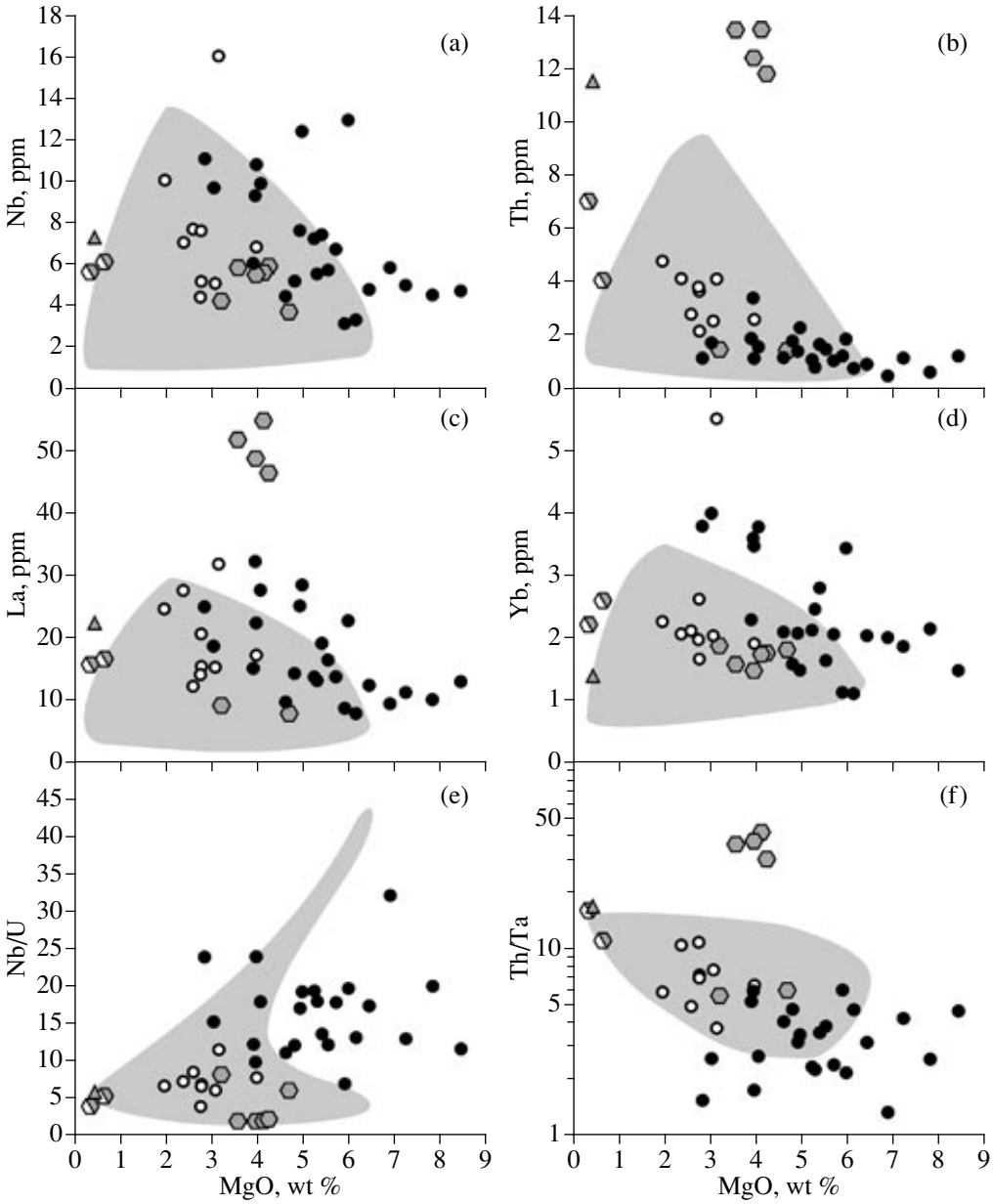

Fig. 8. Variations in the concentration of incompatible trace elements (Nb, Th, La, and Yb) and Nb/U and Th/Ta ratios as functions of MgO content in the basic rocks of the bimodal association of the Noen and Tost ranges and the ACM complex. The shaded fields show the compositions of rocks from the Hercynian basement (our unpublished data). Symbols are the same as in Fig. 3.

istics of subduction-zone melts, including negative Nb and Ta anomalies and a positive Pb anomaly. This suggests that the rocks of a metasomatized mantle wedge played a significant role in their formation (McCulloch and Gamble, 1991; Kelemen et al., 1993, 2003). However, the characteristics of the rift-related basaltoids of the Noen and Tost ranges cannot be assigned to the subduction process only. First, the rift-related rocks were formed in another geodynamic environment corresponding to large-amplitude extension resulting in the formation of dike belts and grabens. Second, these rocks are part of a bimodal association including salic alkaline rocks, which are not characteristics of convergent plate boundary settings. Third, the bimodal association of the Noen and Tost ranges was related to the development of a giant rift system extending over an area of more than 3000×600 km far beyond the subduction zone, and its formation lasted for more than 130 Myr and persisted for a long time after the extinction of the ACM of the northern Asian paleocontinent. Fourth, the rift-related rocks are geochemically different from the basaltoids of the Middle–Late Paleozoic ACM (Figs. 5, 7–9).

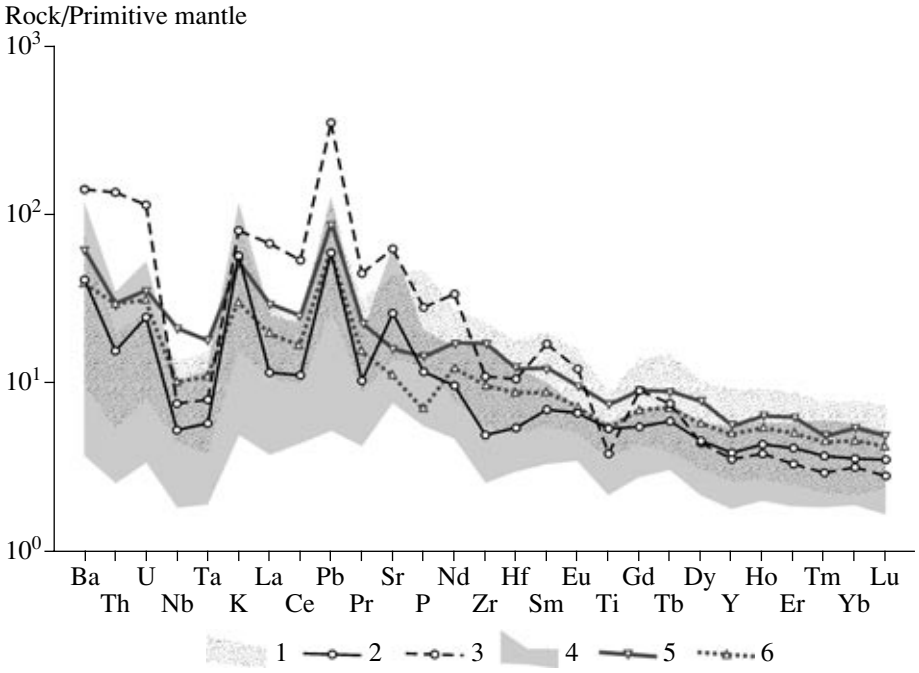

Fig. 9. Primitive mantle normalized (Sun and McDonough, 1989) distribution patterns of incompatible trace elements in the (1) basaltoids of the bimodal association of the Noen and Tost ranges, (2) basalts and trachybasalts of the ACM complex, (3) basaltic trachyandesites and trachyandesites of the ACM complex, and (4) rocks of the Hercynian continental crust. Also shown for comparison are the average compositions of (5) the subalkali basalts of the Siberian trap province (Al'mukhamedov et al., 2004) and (6) Etendeka low-titanium continental flood basalts (Ewart et al., 2004).

A distinguishing feature of the bimodal magmatism of the Gobi–Tien Shan rift zone is the presence of andesites in association with basaltoids. Andesites are practically lacking in other rift zones of the central Asian rift system located in the interior zones of the paleocontinent. The andesites differ from the dominant basaltoids in incompatible element concentrations and ratios and form distinctive correlation relations (Fig. 8). Therefore, the petrogenetic features of basaltoids and andesites should be evaluated separately.

Heterogeneity of Basaltoid Sources

The rift-related basaltoids of the Noen and Tost ranges are geochemically similar to the magmatic occurrences that are undoubtedly connected to mantle plumes. For instance, they resemble the subalkali basalts of the Siberian traps (Al'mukhamedov et al., 2004; Yarmolyuk and Kovalenko, 2003; Fedorenko et al., 1996; Fedorenko, 1997; Farmer, 2003), which also display negative Nb and Ta anomalies, enrichment in K and Pb (Fig. 9), and identical concentrations of incompatible trace elements. This resemblance can be explained by the connection of the magmatism of these two regions to the northern Asian superplume (Yarmolyuk et al., 2000), which controlled the formation of both the central Asian rift system and the traps of the Siberian craton. Rocks geochemically similar to the rift-related basaltoids of the Noen and Tost ranges were documented among the occurrences of plume-related continental magmatism. In particular, the low-titanium basalts of the Etendeka flood volcanic province (Ewart et al., 2004) are similar in trace element concentrations and distribution patterns to the predominant basaltoids of the Noen and Tost ranges relatively depleted in incompatible trace elements (Fig. 9).

The compositional field of rocks of the Hercynian continental crust of southern Mongolia, where the Gobi–Tien Shan rift zone was developed (our unpublished data), is shown in Fig. 9. The rocks are represented by ophiolite and island-arc complexes of both magmatic and sedimentary origin (*Tectonics, Magmatism…*, 2001). The general trace-element distribution patterns of the basaltoids of the bimodal association of the Noen and Tost ranges are identical to those of the basement rocks. The variations of trace-element contents in these associations overlap, although rocks with lower concentrations are more common in the basement complex. In our opinion, this similarity is largely due to the fact that the formation of both the continental crust and the underlying metasomatized rocks of the mantle wedge was related to the development of a subduction zone. The metasomatized sublithospheric mantle was subsequently entrained in the processes of rift-related magmatism as one of its sources. However, in order to explain all the geochemical features of the rift-related basic rocks, other sources must be invoked, including those connected with mantle plume activity. It should be noted that the similarity of the PZ_3–MZ_1

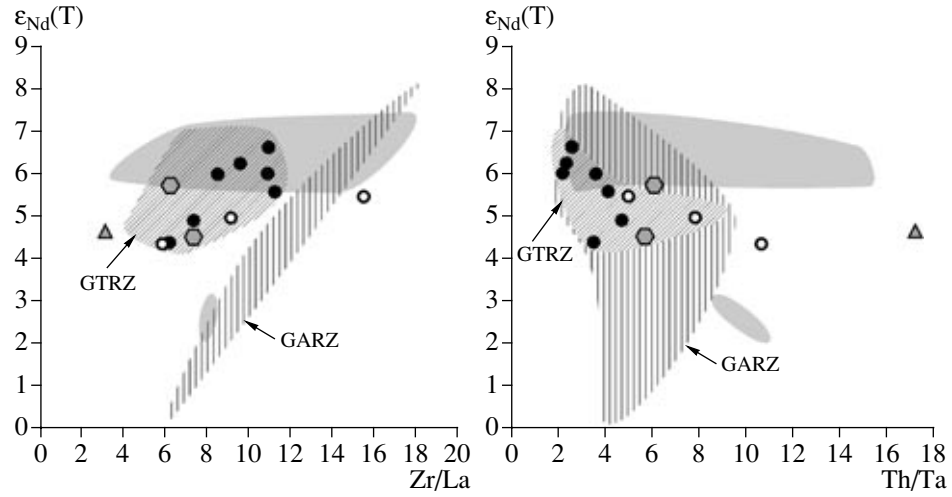

Fig. 10. Neodymium isotopic composition of the basic rocks of the bimodal association of the Noen and Tost ranges as a function of the Zr/La and Th/Ta ratios. Symbols are the same as in Fig. 3.

intraplate magmatism, ACM magmatism, and Hercynian crust-forming magmatism complicates the analysis of contributions from various sources and contaminants to the formation of the rift-related basaltoids of the Gobi–Tien Shan rift zone.

The compositions of rift-related basaltoid of the bimodal association of the Noen and Tost ranges form a linear trend in the $\varepsilon_{Nd}(T)$–$(^{87}Sr/^{86}Sr)_0$ diagram (Fig. 6a), which suggests that at least two isotopically distinct sources took part in the genesis of the rift-related basaltoids of the Noen and Tost ranges: relatively depleted with $\varepsilon_{Nd}(T) > 6.7$ and $(^{87}Sr/^{86}Sr)_0 < 0.70360$ and relatively enriched with $\varepsilon_{Nd}(T) < 4.4$ and $(^{87}Sr/^{86}Sr)_0 > 0.70427$. The same range comprises the isotopic characteristics of basaltoids of another bimodal association occurring 500 km east of the Noen and Tost ranges on the extension of the Gobi–Tien Shan rift zone in the framing of the Haan Bogd peralkaline granite massif, the largest in central Asia (Vladykin et al., 1981; Yarmolyuk et al., 1999; our unpublished data). However, in the other rift zones of the central Asian rift system occurring in the interior parts of the continent, basic rocks have more variable isotopic characteristics (Fig. 6a) extending along the trend of the Noen and Tost basaltoids into the field of more enriched compositions (Yarmolyuk et al., 1999). This allows us to conclude that the rift-related basaltoids of the Gobi–Tien Shan rift zone extending along the margin of the northern Asian paleocontinent were derived from isotopically uniform sources, which were systematically different from the sources of corresponding rocks from the interior parts of the continent.

The isotopic composition of the rift-related basaltoids of the Noen and Tost ranges correlates with some of their geochemical characteristics. For instance, the Nd isotopic composition is negatively correlated with K_2O, Th, U, LREE, Th/Ta, Th/Y, K/Ti, La/Sm, and La/Yb and positively correlated with Nb/U, U/Th, and Zr/La (Fig. 10). Such correlations could not be related to crystallization differentiation and were caused by either the mixing of melt sources, contamination, or a combination of these two processes. However, there are no clear indicators of two-component mixing in the Th/Y–Zr/La, Th/Ta–La/Yb, and other diagrams for the basaltoids. Therefore, we believe that the genesis of rift-related basaltoids of the Noen and Tost ranges involved at least three components, one of which could be represented by the rocks of the Hercynian continental crust and the ACM complex as a contaminant. However, the general similarity of the compositions of the rift-related basaltoids and the basement rocks did not allow us to find reliable geochemical and isotopic indicators of contamination. Nonetheless, we note that the compositions of basaltoids from the Noen and Tost ranges plot somewhat away from the compositional field of the underlying continental crust and form distinctly separate trends (Figs. 8, 10). On the other hand, basaltoids from the central Asian rift zones occurring north of the Gobi–Tien Shan zone and the traps of eastern Siberia, which were formed on an another basement, have identical compositions (Yarmolyuk and Kovalenko, 2000). This indicates the existence of a single mantle source contributing to the formation of all Late Paleozoic–Early Mesozoic basaltoids of the Siberian region. This material was characterized by a high Zr/Hf ratio (38–50 for the basaltoids of the Noen and Tost ranges and 36–54 for the Siberian traps; Al'mukhamedov et al., 2004; Fedorenko et al., 1996; Fedorenko, 1997), higher than those of the basalts of mid-ocean ridges and ocean islands (36; Sun and McDonough, 1989), continental crust (33; Taylor and McLennan, 1988), and the rocks of the Middle–Late Paleozoic ACM of the northern Asian paleocontinent (33–39). The derivation of the basaltoids of the Noen and Tost ranges from a mantle source is also supported

by the high Nb/Ta ratios (14.6–20.5) clustering near the value of typical mantle-related rocks (about 17.5; Green, 1995). Thus, crustal contamination could not be the main reason for the compositional variations of the rift-related basaltoids of the Noen and Tost ranges. With this in mind, we further consider the contributions of various mantle sources.

Rocks with elevated TiO_2 concentrations (1.5–2.78%) were found among the rift-related basaltoids of the Noen and Tost ranges. These rocks have low ratios of K/Ce < 310 (Fig. 11), K/Ti < 1.6 (not shown in the diagram), and K/Nb < 1400 and high P_2O_5 concentrations of 0.45–1.03%. In contrast, the basaltoids with moderate TiO_2 contents (<1.6%) have higher K/Ce (340–720), K/Nb (2400–3800), and K/Ti (1.8–3.2) ratios and lower P_2O_5 concentrations (0.20–0.49%). These two groups of rocks are hereafter referred to as high- and moderate-Ti.

With respect to the above characteristics, the high-Ti basaltoids of the Noen and Tost ranges are similar to mid-ocean ridge basalts (MORB) derived from the depleted mantle and ocean island basalts (OIB) produced by melting of the enriched mantle, which have K/Ce ratios of 86 and 150, K/Ti of 0.1 and 0.9, respectively, and K/Nb of 250 (Sun and McDonough, 1989). Thus, the rift-related high-Ti basaltoids of the Noen and Tost can be regarded as melting products of such an unmetasomatized mantle reservoir. In contrast, the signatures of the moderate-Ti basaltoids are similar to those of the undifferentiated basalts and trachybasalts of the ACM (K/Ce = 470–730, K/Ti = 1.6–2.7, and K/Nb = 2500–4060) and typical island-arc basalts (IAB) showing K/Ce = 350, K/Ti = 1.3, and K/Nb = 3540 (McCulloch and Gamble, 1991). This indicates an important role for the rocks of the metasomatized mantle wedge in the source of the moderate-Ti basaltoids of the Noen and Tost ranges. The considerable variations of Ba/Nb (12–104) and Ba/Ce ratios (2–17) (Fig. 11d) in the basaltoids of the Noen and Tost ranges also suggest the participation of melts from both depleted and/or enriched mantle reservoirs with low Ba/Nb (2 for MORB and 7 for OIB) and Ba/Ce ratios (0.8 for MORB and 4.4 for OIB) and the metasomatized mantle wedge with high Ba/Nb (133 in IAB) and Ba/Ce ratios (13 in IAB).

The appearance of high-Ti basaltoid melts with such characteristics under the conditions of the predominance of metasomatized mantle wedge rocks could only be related to the deep influence of a mantle plume. However, the presence of negative Ta–Nb anomalies in these rocks is not typical of the derivatives of depleted and enriched sources and suggests that the melting of source rocks occurred under water-saturated conditions with the retention of rutile or ilmenite in the residue (Kelemen et al., 1993, 2003). Thus, the geochemical characteristics of the rift-related basaltoids of the Noen and Tost ranges were controlled by the mixing of three sources: the rocks of the metasomatized mantle wedge, depleted mantle, and enriched mantle. Figure 11c illustrates the relationships of these sources in the Th/Y–K/Ce coordinates. Trachybasalt sample NT-1/3 with the maximum K/Ce ratio of 721 can be used as a proxy for the melt derived from the metasomatized mantle wedge. It can be seen, that most of the compositions of rift-related basalts fall within the triangle of mixed melts from these sources. The high-Ti basaltoids plot near the mixing curve of the MORB and OIB sources with a minor contribution from melts formed in the metasomatized mantle. This provides additional evidence for the formation of the high-Ti rift-related basaltoids of the Noen and Tost ranges mainly at the expense of depleted and enriched mantle reservoirs with a minor contribution (no more than 10%) from the metasomatized mantle. The higher role of the metasomatized mantle and variable contributions from the depleted and enriched reservoirs are suggested for the genesis of the moderate-Ti basaltoids.

Phase Composition of the Mantle Protolith

The high- and moderate-Ti basaltoids of the Noen and Tost ranges have different degrees of LREE enrichment relative to HREE. In our opinion, high-LREE/HREE melts are formed by the low-degree melting of the mantle protolith in the garnet stability field, and it is reasonable to suppose that the basic melts of the Noen and Tost ranges were formed at least in part under such conditions.

The Tb/Yb ratio is very sensitive to the presence of garnet in the source and simultaneously not strongly affected by crystal fractionation (Furman et al., 2004). The chondrite-normalized (Sun and McDonough, 1989) $(Tb/Yb)_N$ ratios of melts generated in the garnet stability field must be higher than 1.8 (Wang et al., 2002). Shallower melts equilibrated with a spinel mantle protolith will show lower $(Tb/Yb)_N$ values. According to this criterion, all the rift-related moderate-Ti basaltoids of the bimodal association of the Noen and Tost ranges were formed in the spinel peridotite zone (Fig. 12). Melts equilibrated with both spinel- and garnet-bearing residues were distinguished among the high-Ti basaltoids. Thus, the high-Ti basaltoids, the sources of which were dominated by depleted and enriched mantle rocks, were formed in general at greater depths compared with the moderate-Ti basaltoids derived mainly from the rocks of the metasomatized mantle wedge.

Genesis of Andesites

As was noted above, the occurrence of andesites in the PZ_3–MZ_1 bimodal associations of the central Asian rift system is characteristic only of the Gobi–Tien Shan rift zone. The presence of such rocks in the rift-related association of the Noen and Tost ranges is probably a specific geodynamic feature of rifting of the continental margin. It was shown above that the andesites could not

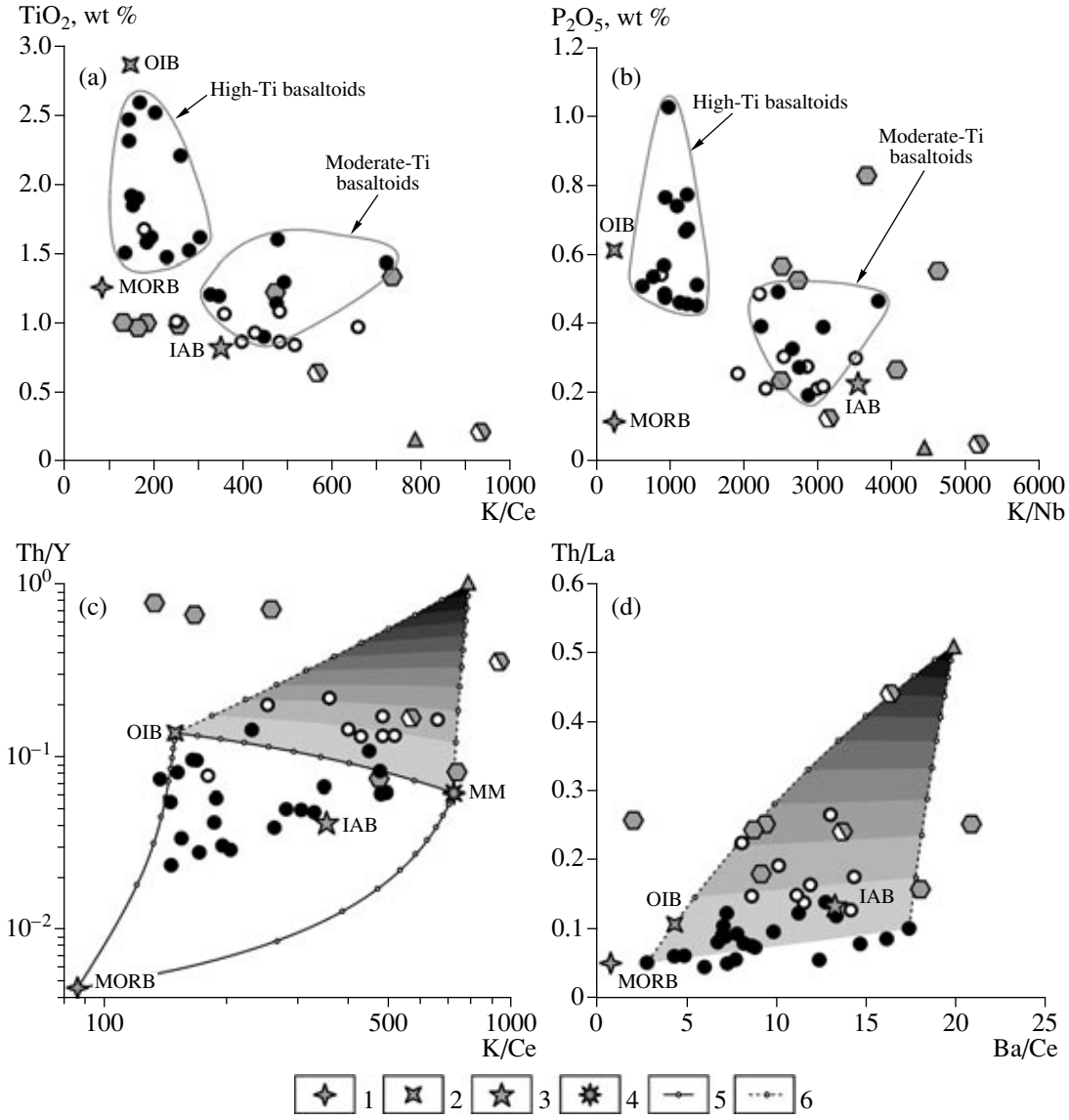

Fig. 11. Diagrams showing the relationships of the sources of the bimodal magmatism of the Noen and Tost ranges. (1)–(3) Model compositions: (1) mid-ocean ridge basalts (MORB), (2) ocean island basalts (OIB) (Sun and McDonough, 1989), (3) island arc basalts (IAB) (McCulloch and Gamble, 1991); (4) composition of melt derived from the metasomatized mantle wedge (MM) (represented by trachybasalt NT-1/3); (5) mixing curve between the melts formed by the melting of depleted and enriched sources and the metasomatized mantle wedge (tick marks are spaced at 10% intervals); and (6) curve corresponding to the assimilation of anatectic granitoid NT-20/21 by basaltoid melts (tick marks and gradient shading correspond to a degree of assimilation of 10%). Other symbols are the same as in Fig.3. See text for further explanation.

be direct derivatives of basaltoid melts, and consequently, their compositional features require a relatively SiO_2-rich and low-MgO source or a contaminant with higher Th/La, Th/Y, and Th/Ta and lower Nb/U, Nb/Th, and Nb/Ta ratios compared with the basaltoids. Such characteristics, including the lower Nb/Ta ratios of the andesites (12.9–17.6) relative to the basaltoids (15.1–20.5), suggest a possible contribution from the continental crust, which has an Nb/Ta ratio of about 11–12 (Green, 1995) or contamination with crustal granitoids. Because of this, we consider the genesis of andesites using the model of the contamination of rift-related basaltoids with the rocks underlying the bimodal association of the Noen and Tost ranges or melts derived from them.

With respect to geochemical characteristics (Fig. 8) and Nd isotope ratios (Fig. 10), almost all andesites fall into the field of rocks from the Hercynian continental crust, which forms a basement for the continental-margin and rift-related magmatism. In the isotopic diagrams, their compositions plot between the fields of Hercynian volcanic rocks with $\varepsilon_{Nd}(T) > 5.7$ and sedimentary rocks with $\varepsilon_{Nd}(T) < 3.1$. The andesites are enriched in the heavy oxygen isotope ($\delta^{18}O = 6.3–8‰$)

relative to the basaltoids (Fig. 6b), i.e., they are shifted toward the basement rocks showing $\delta^{18}O > 10.7‰$. This allows us to suggest the contamination of rift-related basaltoid melts mainly by the SiO_2-rich and low-MgO sedimentary rocks of the basement with low $\varepsilon_{Nd}(T)$ values. This process must produce rocks with SiO_2 contents higher than those in the basaltoids. This raises the question why such contaminated rocks are lacking in other rift zones of the central Asian rift system (Yarmolyuk et al., 1999; Yarmolyuk and Kovalenko, 2000). It is conceivable that the contamination of the rift-related basaltoids of the Gobi–Tien Shan rift zone was assisted by the generally higher heat flow at the margin of the paleocontinent, which was related to the development of the area in the ACM regime immediately before the onset of rifting.

The contamination of mantle magmas might also be related to the specific geodynamic conditions at the continental margin, which included extensive crustal anatexis under the influence of mantle melts. This process produced some granitoid massifs of normal alkalinity. They were formed synchronously with the bimodal magmatism, probably during compression episodes occurring from time to time in the complex geodynamic setting. In particular, such a biotite granite massif was formed in the western part of the Tost Range (Fig. 2) between two episodes of peralkaline granitoid emplacement in the zone of the dike belt. The basaltoids that initiated crustal anatexis could assimilate in part the molten material changing their composition to andesite.

The isotopic compositions of the rocks are consistent with this model. The biotite granites are enriched in the heavy oxygen isotope ($\delta^{18}O = 9.3‰$) relative to the rift-related basaltoids. When basaltoids with normal mantle characteristics assimilate granitoid melts, they become enriched in ^{18}O, and andesites formed in such a way must have heavy oxygen isotope compositions (Fig. 6b). The Nd and Sr isotope compositions of the biotite granites of the Tost Range, $\varepsilon_{Nd}(T) = 4.7$ and $(^{87}Sr/^{86}Sr)_0 = 0.70421$, plot at the lower end of the trend formed by the rift-related basaltoids (Fig. 6a), and these parameters are therefore not very sensitive to granitoid melt assimilation. However, the fact that the Sr and Nd isotopic compositions of the andesites are also confined to the relatively enriched in radiogenic Sr and depleted in radiogenic Nd part of the trend of the rift-related basaltoids of the Noen and Tost ranges is compatible with the model of the contamination of basaltoid magmas with biotite granite melts.

The geochemical characteristics of the andesites of the Noen and Tost ranges can be best explained by the hypothesis of the assimilation of anatectic crustal melts by basaltoid magmas. The trends of the assimilation of granitoid melt NT-20/21 by the end-members of the basaltoid series of the Noen and Tost ranges are shown in Figs. 11c and 11d, from which it is clear that the maximum degree of assimilation was 30%. However,

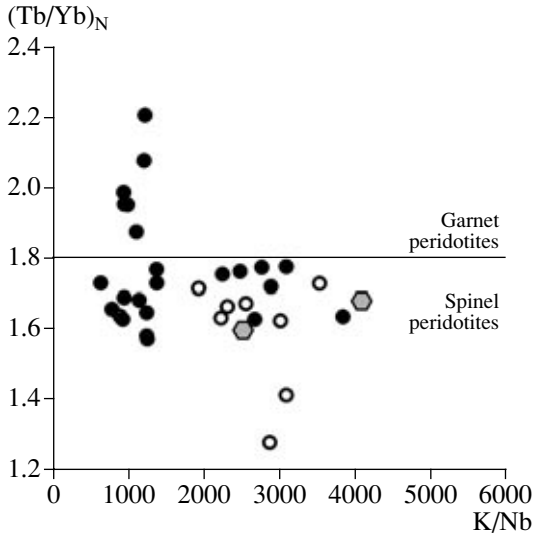

Fig. 12. Chondrite-normalized (Sun and McDonough, 1989) $(Tb/Yb)_N$ ratio as a function of K/Nb for the basaltoids and andesites of the bimodal association of the Noen and Tost ranges illustrating the composition of the mantle protolith. The boundary between garnet and spinel peridotites is after Wang et al. (2002). Symbols are the same as in Fig. 3.

such numerical estimates are associated with considerable uncertainties, taking into account the general heterogeneity of the sources of basaltoids and granitoids and crystal fractionation processes, which obviously affected the compositions of rift-related rocks.

Another possible high-SiO_2 and low-MgO contaminant for the rift-related rocks of the Noen and Tost ranges is the dacites and rhyolites of the ACM complex. Their geochemical characteristics are similar to those of biotite granites, and contamination with these rocks and anatectic granitoids will exert similar effects on the compositions of rift-related basaltoid melts.

Thus, the andesites of the bimodal association of the Noen and Tost ranges could be formed from basaltoid melts by the assimilation of either the rocks of the Hercynian continental crust dominated by sediments, anatectic granitoid melts, or silicic rocks of the ACM complex. These three models are similar in terms of the estimation of the composition of assimilated material, because both the anatectic granitoids and dacites and rhyolites of the ACM complex were formed under the influence of the continental crustal rocks. Thus, the andesites of the Noen and Tost ranges can be considered as products of crustal contamination.

Unfortunately, the currently available data and models for the rift-related basic rocks of the bimodal association of the Noen and Tost ranges allow only qualitative reconstructions of the contributions of sources, contamination, crystal fractionation, and melting conditions of the protolith, because the geochemical results of these processes overlap each other.

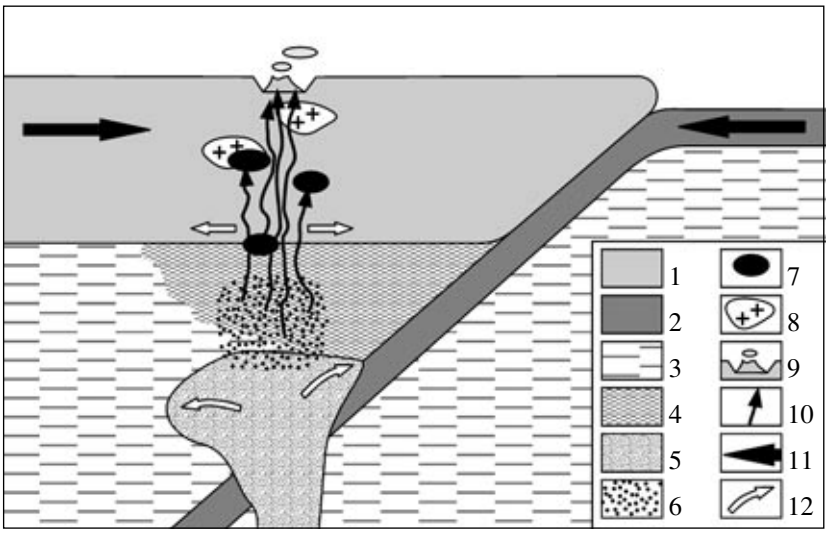

Fig. 13. Geodynamic model of rift formation in an active continental margin and relationships of magma sources. (1) Continental crust, (2) oceanic crust, (3) depleted mantle, (4) metasomatized mantle wedge, (5) enriched plume mantle, (6) magma formation zone, (7) transitional magma chamber, (8) anatectic granitoid, (9) graben of the rift zone, (10) ascending mantle magma, (11) direction of compression stress related to subduction, and (12) direction of tensional stresses related to the mantle plume.

GEODYNAMIC CONDITIONS OF THE RIFT-RELATED MAGMATISM OF THE NOEN AND TOST RANGES

The geodynamic interpretation of continental rift zones with alkaline basic or bimodal magmatism usually invokes the ascent of mantle plumes and their interaction with the continental lithosphere (Rogers et al., 2000; Peccerillo et al., 2003; Trua et al., 1999; Macdonald et al., 2001; Fedorenko et al., 1996; Fedorenko, 1997; etc.). The Late Paleozoic–Early Mesozoic rift system of central Asia is not an exception. Its prolonged development from the end of the Carboniferous to the beginning of the Jurassic is explained by the overriding of a large mantle plume by the margin of the Siberian paleocontinent (Yarmolyuk et al., 1999, 2000; Yarmolyuk and Kovalenko, 2003). In the early Late Paleozoic, the southern folded framing of the Siberian craton was an extended zone with continental margin magmatism related to the subduction of the oceanic plate beneath the drifting continent (Gordienko, 1987; *Tectonics, Magmatism…*, 2001). After the cessation of subduction magmatism, rifting processes began in response to the overriding of the continental lithosphere over a mantle hot spot, which was previously located within the paleo-Asian Ocean. Within the time interval 320–190 Ma, the zone of active rifting moved into the continent forming the rift zones of the Gobi–Tien Shan, main Mongolian lineament, Gobi–Altai, northern Mongolia, and western Transbaikalia.

The geochemical and isotopic variations in the basic rocks of the rift-related bimodal association of the Noen and Tost ranges suggest that the magma generation was connected with three sources with the characteristics of depleted and enriched mantle reservoirs and a metasomatized mantle wedge. The contribution from these three sources is consistent with the proposed geodynamic model (Fig. 13). When an ascending mantle plume with the geochemical characteristics of the enriched mantle appeared directly beneath the margin of the continent, the initial stage of its thermal influence caused partial melting in the depleted mantle and the overlying metasomatized mantle wedge. The further heating of the mantle wedge by the plume provided conditions for the transportation of enriched deep-derived material to the surface.

CONCLUSIONS

The geologic structure and geochemical characteristics of the basaltoids and andesites of the Noen and Tost ranges of the Gobi–Tien Shan rift zone of southern Mongolia allowed us to determine some specific features of rift-forming processes occurring in an active continental margin. The rift origin of the magmatism of the Noen and Tost ranges is suggested primarily by the geologic structure of magmatic associations. First, these volcanic rocks are confined to a narrow (no wider than 40 km) long (more than 200 km) graben, which is part of a chain of coeval grabens and intrusive massifs extending over more than 3000 km along the margin of the paleocontinent. Second, the volcanic rocks of the graben are accompanied by dike belts indicating a large-scale extension setting. Third, the volcanic and dike rocks are represented by the bimodal association, including basaltoids, peralkaline rhyolites, and peralkaline granites with a very minor amount of trachytes. Such associations are characteristic of intracontinental rift zones and distinguish rift-related complexes from the products of continental margin volcanism, which

are widespread in the structure of the central Asian orogenic belt.

The geochemical characteristics of the rift-related basaltoids of the Noen and Tost ranges are not typical of the rocks formed in intracontinental rift zones. The basaltoids show negative Ta and Nb anomalies and positive K and Pb anomalies, which are characteristic of rocks from a convergent plate boundary environment. With respect to these parameters, they are similar to the underlying rocks of the Hercynian basement and the ACM volcanic rocks of the northern Asian paleocontinent. Considerable variations in the concentrations and ratios of some major and incompatible trace elements and Sr, Nd, and O isotope characteristics of the rift-related basaltoids allowed us to distinguish relatively high- and moderate-Ti rocks, which were formed under the influence of three mantle sources: a depleted mantle reservoir similar to the sources of mid-ocean ridge basalts, an enriched mantle reservoir similar to the source of ocean island basalts, and a metasomatized mantle wedge. The source of the high-Ti rocks was dominated by the depleted and enriched mantle reservoirs, and the moderate-Ti melts were formed mainly at the expense of the rocks of the metasomatized mantle wedge. The moderate-Ti rift-related basaltoids were derived from spinel peridotites, and the high-Ti basaltoids, from both spinel and garnet peridotites.

The similarity and differences of the rift-related and subduction (Hercynian basement and Middle–Late Paleozoic ACM) associations were controlled by the geodynamic conditions of their formation. The rocks of the Hercynian continental crust and the northern Asian ACM were formed in a suprasubduction setting with regional compression accompanied by periodic ejection of variably differentiated melts from magma chambers. In contrast, the rift-related magmatism was formed under extensional conditions above a mantle hot spot. The mantle plume that initiated rifting interacted directly below the continental margin with the rocks of the metasomatized mantle wedge and depleted mantle causing their melting. Under such conditions only small amounts of deep enriched material from the mantle plume could reach the surface. Basic magmas could erupt only from subcrustal magma chambers. When they did not reach the surface and ponded within the continental crust, they initiated anatexis processes and could in part assimilate the enclosing material or melt derived from it.

ACKNOWLEDGMENTS

This study was financially supported by the Russian Foundation for Basic Research (project nos. 05-05-64001, 05-05-64000, and 05-05-64056), Program for the Support of Leading Scientific Schools (grant no. NSh-1145.2003.5), and programs of fundamental research nos. 5, 7, and 8 of the Earth Science Division, Russian Academy of Sciences.

REFERENCES

1. A. I. Al'mukhamedov, A. Ya. Medvedev, and V. V. Zolotukhin, "Chemical Evolution of the Permian–Triassic Basalts of the Siberian Platform in Space and Time," Petrologiya **12**, 339–353 (2004) [Petrology **12**, 297–310 (2004)].
2. F. Barberi, G. Ferrara, R. Santacrose, et al., "Transitional Basalt–Pantellerite Sequence of Fractional Crystallization, the Boina Centre (Afar Rift, Ethiopia)," J. Petrol. **16**, 22–56 (1975).
3. L. Civetta, M. D'Antonio, G. Orsi, and G. R. Tilton, "The Geochemistry of Volcanic Rocks from Pantelleria Island, Sicily Channel: Petrogenesis and Characteristics of the Mantle Source Region," J. Petrol. **39**, 1453–1491 (1998).
4. G. R. Davies and R. Macdonald, "Crustal Influences in the Petrogenesis of the Naivasha Basalt–Comendite Complex: Combined Trace Element and Sr–Nd–Pb Isotope Constraints," J. Petrol. **28**, 1009–1031 (1987).
5. A. Ewart, J. S. Marsh, S. C. Milner, et al., "Petrology and Geochemistry of Early Cretaceous Bimodal Continental Flood Volcanism of the NW Etendeka, Namibia. Part 1: Introduction, Mafic Lavas and Re-Evaluation of Mantle Source Components," J. Petrol. **45**, 59–105 (2004).
6. G. L. Farmer, "Continental Basaltic Rocks," in *Treatise on Geochemistry*, Ed. By L. R. Rudnick (Elsevier, 2003), Vol. 3, pp. 85–121.
7. V. A. Fedorenko, "Results of New Field and Geochemical Studies of the Volcanic and Intrusive Rocks of the Maymecha–Kotuy Area, Siberian Flood Basalt Province, Russia," Int. Geol. Rev. **39**, 353–479 (1997).
8. V. A. Fedorenko, P. C. Lightfoot, A. J. Naldrett, et al., "Petrogenesis of the Flood-Basalt Sequence of Norilsk, North Central Siberia," Int. Geol. Rev. **38**, 99–135 (1996).
9. T. Furman, J. G. Bryce, J. Karson, and A. Iotti, "East African Rift System (EARS) Plume Structure: Insights from Quaternary Mafic Lavas of Turkana, Kenya," J. Petrol. **45**, 1069–1088 (2004).
10. I. V. Gordienko, *Paleozoic Magmatism and Geodynamics of the Central Asian Fold Belt* (Nauka, Moscow, 1987) [in Russian].
11. T. H. Green, "Significance of Nb/Ta as an Indicator of Geochemical Processes in the Crust–Mantle System," Chem. Geol. **120**, 347–359 (1995).
12. P. B. Kelemen, K. Hanghoj, and A. R. Greene, "One View of the Geochemistry of Subduction-Related Magmatic Arcs, with an Emphasis on Primitive Andesite and Lower Crust," in *Treatise on Geochemistry*, Ed. By R. L. Rudnick (Elsevier, 2003), Vol. 3, pp. 593–659.
13. P. B. Kelemen, N. Shimizu, and T. Dunn, "Relative Depletion of Niobium in Some Arc Magmas and the Continental Crust: Partitioning of K, Nb, La and Ce during Melt/Rock Reaction in Upper Mantle," Earth Planet. Sci. Lett. **120**, 11–134 (1993).
14. E. M. Klein, "Geochemistry of the Igneous Oceanic Crust," in *Treatise on Geochemistry*, Ed. By R. L. Rudnick (Elsevier, 2003), Vol. 3, pp. 433–463.
15. V. I. Kovalenko, V. V. Yarmolyuk, E. B. Sal'nikova, et al., "Sources of Igneous Rocks and Genesis of the Early Mesozoic Tectonomagmatic Area of the Mongolia–Transbaikalia Magmatic Region: 2. Petrology and

Geochemistry," Petrologiya **11**, 227–254 (2003) [Petrology **11**, 205–229 (2003)].

16. A. M. Kozlovsky, V. V. Yarmolyuk, E. B. Sal'nikova, et al., "Age of Bimodal and Alkali Granite Magmatism of the Gobi–Tien Shan Rift Zone, Tost Range, Southern Mongolia," Petrologiya **13**, 232–239 (2005) [Petrology **13**, 197–204 (2005)].
17. M. J. Le Bas, R. W. Le Maitre, A. Streckeisen, and B. A. Zanettin, "Chemical Classification of Volcanic Rocks Based on the Total Alkali–Silica Diagram," J. Petrol. **27**, 745–750 (1986).
18. R. Macdonald, N. W. Rogers, J. G. Fitton, et al., "Plume–Lithosphere Interactions in the Generation of the Basalts of the Kenya Rift, East Africa," J. Petrol. **42**, 877–900 (2001).
19. M. T. McCulloch and J. A. Gamble, "Geochemical and Geodynamical Constraints on Subduction Zone Magmatism," Earth Planet. Sci. Lett. **102**, 358–374 (1991).
20. H. Palme and H. St. C. O'Neill, "Cosmochemical Estimates of Mantle Composition," in *Treatise on Geochemistry*, Ed. by R. W. Carlson (Elsevier, 2003), Vol. 2, pp. 1–38.
21. A. Peccerillo, M. R. Barberio, G. Yirgu, et al., "Relationships between Mafic and Peralkaline Silicic Magmatism in Continental Rift Settings: A Petrological, Geochemical and Isotopic Study of the Gedemsa Volcano, Central Ethiopian Rift," J. Petrol. **44**, 2003–2032 (2003).
22. B. G. Pokrovskii, *Crustal Contamination of Mantle Magmas* (Nauka, Moscow, 2000) [in Russian].
23. N. Rogers, R. Macdonald, J. G. Fitton, et al., "Two Mantle Plumes beneath the East African Rift System: Sr, Nd and Pb Isotope Evidence from Kenya Rift Basalts," Earth Planet. Sci. Lett. **176**, 387–400 (2000).
24. V. M. Savatenkov, I. M. Morozova, and L. K. Levskii, "Behavior of the Sm–Nd, Rb–Sr, K–Ar, and U–Pb Isotopic Systems during Alkaline Metasomatism: Fenites in the Outer-Contact Zone of an Ultramafic–Alkaline Intrusion," Geokhimiya, No. 10, 1027–1049 (2004) [Geochem. Int. **42**, 899–920 (2004)].
25. S. S. Sun and W. F. McDonough, "Chemical and Isotopic Systematics of Oceanic Basalts: Implications for Mantle Composition and Processes," in *Magmatism in the Ocean Basins*, Ed. by A. D. Saunders and M. J. Norry, Geol. Soc. London Spec. Publ. **42**, 313–346 (1989).
26. S. R. Taylor and S. M. McLennan, *The Continental Crust: Its Composition and Evolution* (Blackwell, Oxford, 1985; Mir, Moscow, 1988).
27. *Tectonics, Magmatism, and Metallogeny of Mongolia*, Ed. by A. B. Dergunov (Routledge, London and New York, 2001).
28. T. Trua, C. Daniel, and R. Mazzuoli, "Crustal Control in the Genesis of Plio-Quaternary Bimodal Magmatism of the Main Ethiopian Rift (MER): Geochemical and Isotopic (Sr, Nd, Pb) Evidence," Chem. Geol. **155**, 201–231 (1999).
29. N. V. Vladykin, V. I. Kovalenko, and M. D. Dorfman, *Mineralogical and Geochemical Features of the Haan Bogd Alkaline Granitoid Massif, Mongolia* (Nauka, Moscow, 1981) [in Russian].
30. K. Wang, T. Plank, J. D. Walker, and E. I. Smith, "A Mantle Melting Profile across the Basin and Range, SW USA," J. Geophys. Res. **107** (B1), 10.1029/2001JB000209 (2002).
31. V. V. Yarmolyuk, *Upper Paleozoic Volcanogenic Associations and Structural–Petrological Features of Their Evolution* (Nauka, Moscow, 1978) [in Russian].
32. V. V. Yarmolyuk, *Late Paleozoic Volcanism in the Continental Riftogenic Structures of Central Asia* (Nauka, Moscow, 1983) [in Russian].
33. V. V. Yarmolyuk and V. I. Kovalenko, *Rift-Related Magmatism of Active Continental Margins and Its Ore Potential* (Nauka, Moscow, 1991) [in Russian].
34. V. V. Yarmolyuk and V. I. Kovalenko, "Geochemical and Isotopic Characteristics of the Anomalous Mantle of Northern Asia in the Late Paleozoic–Early Mesozoic: Data on Intraplate Mafic Magmatism," Dokl. Akad. Nauk **375**, 525–530 (2000) [Dokl. Earth Sci. **375A**, 1427–1432 (2000)].
35. V. V. Yarmolyuk and V. I. Kovalenko, "Deep Geodynamics and Mantle Plumes: Their Role in the Formation of the Central Asian Fold Belt," Petrologiya **11**, 556–586 (2003) [Petrology **11**, 504–533 (2003)].
36. V. V. Yarmolyuk, M. V. Durante, V. I. Kovalenko, et al., "Age of the Comendite–Alkali Granite Association of Southern Mongolia," Izv. Akad. Nauk SSSR, Ser. Geol., No. 9, 40–48 (1981).
37. V. V. Yarmolyuk, V. S. Samoilov, V. G. Ivanov, et al., "Composition and Sources of Basalts in the Late Paleozoic Rift System of Central Asia: Geochemical and Isotopic Data," Geokhimiya, No. 10, 1027–1042 (1999) [Geochem. Int. **37**, 921–935 (1999)].
38. V. V. Yarmolyuk, V. I. Kovalenko, and M. I. Kuz'min, "North Asian Superplume Activity in the Phanerozoic: Magmatism and Geodynamics," Geotektonika, No. 5, 3–29 (2000) [Geotectonics **34**, 343–366 (2000)].